1.4 Pileup Measurements and Modelling

1.4.1 Introduction

In the low flux limit x-rays incident on a CCD are assumed to be independently detectable. That is, the detection of any one x-ray is not affected by the x-ray flux incident on the detector. At sufficiently high flux this approximation breaks down as "pileup" occurs. In a CCD the piled-up x-rays do not directly interact with each other, but their electron charge clouds, which form in the depleted region of the CCD, merge or even overlap. All isolated x-rays produce charge clouds whose detection pattern varies strongly with (1) the x-ray energy, (2) the sub-pixel location of the initial photoelectric interaction, (3) the depth of the interaction, and (4) the detector electronics. All detections, or events, can be categorized by (1) the shape (grade) and (2) the magnitude (energy) of their charge cloud pattern. Figure 1.20 represents a matrix of the possible grade-energy combinations for which a single x-ray can be detected. The x-ray counts for a timed exposure will divide among the categories. In the low flux limit, the probability of a single x-ray to produce an event in any category approaches a "pileup-free" value characterisitic of the detector and the spectral content of the source. However, the probability of producing an event in any category is a function of the incident flux, and the the essential problem of pileup characterization is to determine this functional relationship. The effect of pileup is to redistribute the counts in each category, as exemplified by the arrows in the figure.

The largest effect of merging charge clouds is to reduce the number of detected "good" x-ray events. Here by "good" we mean that the event satisfies both of the following conditions: i) the event amplitude is in the spectral band of interest and ii) that the event grade (shape) is in the grade set of interest. The merged cloud resulting from pileup will most likely be detected as a single x-ray event with either a different grade (e.g. if the two x-rays landed in adjacent pixels) or a different energy (e.g. if the two x-rays landed in the same pixel). Many cases will appear as mixtures of these types of pileup. In either case, as a second good x-ray event is produced near a first good x-ray event, not only is the second event undetected, but the first x-ray is removed from detection as a good event. These major redistributions are represented by the heavy arrows in Fig. 1.20. The smaller redistributions shown by the light arrows occur very infrequently for quasi-monochromatic x-ray beams and are not considered here.

There are two complications in a general pileup analysis. The first concerns spatial distribution of the incident flux. We note that, in general, pileup effects are a function of fluence (number of events per unit area within a given CCD readout or exposure), and if the incident fluence varies with position on the detector, the pileup effects will also vary. Thus, in general, pileup can change the apparent spatial distribution of detected flux. In particular, the apparent HRMA/ACIS point-response function can be changed by pileup effects. The discussion in this section is based on experimental data with uniform illumination, and we do not specifically address effects of pileup on the point response function. We note, however, that the pileup "cross-sections" we report below are prerequisites for understanding the effects of pileup on spatial flux distribution measurements. A short discussion at the end of this section considers some aspects of pileup in the limit of a perfectly focussed point source.

The second complication for pileup analysis is the spectral distribution of the incident flux. Here there are two limits, those of a monochromatic source and a continuum source, respectively. The strategy followed in this discussion is to examine a monochromatic source first to understand the redistribution of events as a function of energy. Then, an approximation technique will be discussed to apply these results to a more general spectral distribution.

The remainder of this section is organized as follows. The next subsection details a simple pileup model for a quasi-monochromatic source. This approach only considers the effect of pileup on the number of detected counts at one major line in the spectrum. The strategy is to develop a theory based on fundamental pileup processes which can be applied for any CCD. The following subsection describes pileup experiments which when analyzed in the context of the preceeding theory provide generally applicable cross sections for pileup processe as a function of incident X-ray energy. The final section extends the simple model to include any arbitrary spectrum, specifically including spectral redistribution.

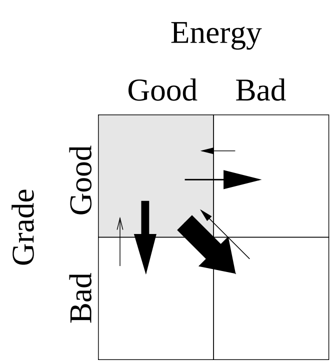

Figure 1.20: Possible redistributions of detected x-rays due to pileup

1.4.2 Simple model of pileup for a quasi-monochromatic incident spectrum

The simple model starts by defining any x-ray event detected with the desired energy and grade to be "good". All other events (i.e., those with different energy or grade) are defined as "bad". Most practical x-ray line sources are not monochromatic, and are typically a mixture of a monochromatic line, other spectral features, and some continuum. The pileup model quantifies this aspect by defining that for every "good" x-ray event there are α "bad" events. Alternatively, if, in the absence of pileup, the number of good incident x-rays is N_i out of a total number of events N_T, then the fraction f_B of good x-ray events is $f_B = N_i/N_T = 1/(1+\alpha)$. This model of a quasi-monochromatic beam is a good representation of the x-ray sources used in the ACIS quantum efficiency calibration.

Although for any CCD exposure the time history of event interactions is unknown, for the purposes of analysis we can picture the x-rays incident in one exposure as striking the CCD serially. The goal is to describe a function $N_d(N_i)$ which represents the number of detected good x-rays as a function of the number of incident good x-ray events. By inverting this function, we can determine N_i from an experimental measurement of N_d. We begin construction of this function by examining the effect of a single x-ray.

Let ϵ be the effective area of the CCD affected by the occurrence of a "good" x-ray event (typically the desired energy is that of a K_α line the desired shapes are ASCA grades 0,2,3,4,and 6). In general, $\epsilon = \epsilon(E)$ will be a function of energy; the energy dependence is described in detail later. Similarly, ϵ' is the average effective area corresponding to any other x-rays, i.e. those with different energies and grades. The physical meaning of ϵ is that if a second x-ray is absorbed near a prior x-ray event such that the center of the second photoelectric absorption occurs within the area ϵ centered on the first x-ray, then an interaction occurs. Specific interaction effects are described mathematically below. We can derive the minimum size for ϵ commensurate with our event detection criteria. All (standard) event discrimination is based on the 3x3 pixel subarray surrounding a local maximum of detected charge. Thus, any second x-ray landing within the subarray invokes an interaction, and the area of 9 pixels forms a lower limit for ϵ. In all that follows, we express ϵ and ϵ' in units of the area of one quadrant of an ACIS CCID17 detector. In these units, a nine-pixel "island" has an area of 3.4×10^{-5}.

The mathematical model begins by schematically dividing the area of a CCD as shown in Fig. 1.21. In our units, the total surface area of the detector (one quadrant of a CCID17) is normalized to unity. Let A_1 be the total area occupied by all good x-ray events (A_1 can also be interpreted as a probability or cross section for interaction; however the interpretation as an area is useful for developing a model). The number of detected events is taken to be $N_d = A_1/\epsilon$. This assumption is approximate since two good x-ray events

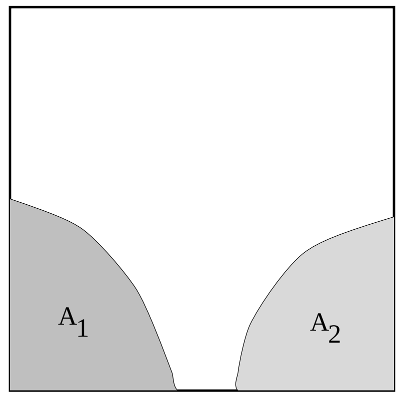

Figure 1.21: Regions of CCD for pileup model

could lie close enough together so that their ϵs overlap while they do not interact. Let A_2 be the total area occupied by charge produced by all other events. Then $1 - A_1 - A_2$ is the CCD area unblemished by any interaction. The probability for an incident x-ray to land on a previous good x-ray event is A_1; the probability for an incident x-ray to land on a previous bad x-ray event is A_2, and the probability for an incident x-ray to land and be detected in unperturbed pixels is $1 - A_1 - A_2$. The effect of an incident x-ray landing in A_1 is removal of one previous x-ray from A_1 while adding some area ϵ'' to A_2, which must be between 1 and 2 times ϵ. We assume that any x-ray landing in A_2 does not change either A_1 or A_2. Finally, we assume that A_1 can increase only by good interactions in the unperturbed region $1 - A_1 - A_2$. Then the change of A_1 and A_2 with per unit change in N_i can be described by the following pair of ordinary differential equations:

$$\frac{dA_1}{dN_T} = (1 - A_1 - A_2) f_B \epsilon - A_1 \epsilon \tag{1.9}$$

$$\frac{dA_2}{dN_T} = (1 - A_1 - A_2)(1 - f_B)\epsilon' + A_1 \epsilon'' \tag{1.10}$$

The solution is obtained by combining the two equations to separate variables. This results in a second order differential equation with the following solution,

$$A_1 = \epsilon/\beta exp(-\hat{\epsilon}N_i)sin(\beta N_i) \tag{1.11}$$

or

$$N_d = f_B N_T e^{-\hat{\epsilon} f_B N_T} sinc(f_B \beta N_T) \tag{1.12}$$

where

$$\hat{\epsilon} = \epsilon \left[1 + \alpha(1 + \epsilon^{'}/\epsilon)\middle/ 2\right], \tag{1.13}$$

$$\beta = \sqrt{(1+\alpha)(\alpha\epsilon\epsilon' + \epsilon\epsilon'') - \hat{\epsilon}^2} \tag{1.14}$$

and

$$A_1 = \epsilon N_d, f_B = N_i/N_T \tag{1.15}$$

Equation 1.12 has the desired asymtotic limit of $N_i = N_d$ for low flux, with the following useful expansion for the logarithm of the ratio:

$$log(\frac{N_d}{N_i}) = -\hat{\epsilon}N_i - \beta^2 N_i^2/6 \tag{1.16}$$

In the limit where $\epsilon^{'} \sim \epsilon$ and $\epsilon^{''} \sim 3/2\epsilon$ then

$$\beta = \hat{\epsilon}/\sqrt{2(1+\alpha)}$$

Solutions to Eqn. 1.12 are plotted in Fig. 1.22 for two different flux ranges and for $\hat{\epsilon}$=0,2,4,...40 (x10^5) using $\epsilon^{''} = 3/2\epsilon$. Specifically, the cross-section $\hat{\epsilon}$ equals the fractional area of a CCD region of interest, and N_d and N_i are the corresponding counts in that region. Note that $\hat{\epsilon} = 10 \times 10^{-5}$ corresponds to a area of 26.2 pixels. The deviation from the line $N_i = N_d$ increases as $\hat{\epsilon}$ increases. All the curves bend over for significantly high pileup and should assymtote to 0 for high enough N_i. This high pileup limit corresponds to severe charge cloud overlap so that very few x-rays satisfy the event selection criteria.

1.4.3 Pileup experiments and determination of $\hat{\epsilon}$ and ϵ

The experimental technique to measure ϵ and $\hat{\epsilon}$ used the High Energy X-ray Source (HEXS) at MIT's CCD Calibration Facility. HEXS is the same source used for the ACIS quantum efficiency calibration, so careful measurements of pileup using that source are particularly important for the AXAF program. The HEXS source uses fluorescence from 12 different targets ranging from Al to Ge as shown in Table 1.20. The fluorescence spectrum is generated by the bremsstrahlung spectrum from a commercial electron impact x-ray tube using a Mo target. The tube current and voltage are independently adjustable and are temporally stable to within one percent over relevant measurement periods. The maximum tube power is 9 W, with a maximum voltage of 30 kV.

Target	Energy	X-ray mfp in Si
	(eV)	μm
Al	1487	8.0
Si	1740	12.4
P	2015	1.6
Cl	2622	3.1
Ti	4508	13.6
V	4949	17.7
Fe	6399	36.9
Co	6925	46.4
Ni	7471	57.8
Cu	8040	71.6
Zn	8630	88.0
Ge	9874	130.7

Table 1.20: HEXS targets, energies, and x-ray penetration depths.

All detectors used for this analysis are flight-like ACIS CCDID-17s, produced by MIT Lincoln Laboratories, which have a 1024 column by 1026 row array of 24 μm square pixels. As mentioned above, each CCD is divided into 4 readout quadrants of 256x1026 pixels. Since the gain from each quadrant can be different, most analysis is conducted on a quadrant basis rather than on the entire CCD. Each CCD was flight qualified for ACIS although only w140c4r was selected for the flight focal plane.

A series of 11 pileup measurements were conducted using various CCDs, HEXS configurations, electronics and exposure times. The different configurations are listed in Table 1.21 . For each configuration, the CCD was exposed to x-rays from most of the 12 available targets. For each target, a sequence of exposures was taken with 4 or 5 different x-ray fluxes generated by using different tube currents (the tube voltage was held constant at 15 kV). The range of fluxes covered an approximately even spread up to twice the nominal flux used during the ACIS calibration.

An important assumption for the process is that the x-ray flux from HEXS varies linearly

CCD	Date	Electronics	Exposure Time	Comments
w103c4	03jun96	Lbox	7.22	Early HEXS configuration
w103c4	16jan97	Lbox	7.22	
w103c4	12feb97	Lbox	7.22	
w140c4r	22jan97	DEA	3.28	Back sided CCD
w163c3	27sep96	DEA	3.28	
w190c3	26nov96	DEA	3.28	
w203c2	07may97	DEA	3.28	
w203c2	08may97	DEA	7.15	Lbox exposure time
w203c4r	16jan97	DEA	3.28	
w210c3r	12may97	DEA	3.28	
w210c3r	12may97	DEA	7.15	Lbox exposure time

Table 1.21: Pileup measurement configurations.

with the x-ray tube current. This was checked two different ways. First, the actual tube current was measurered using three different current meters and compared to the front panel display. All agreed within error. Secondly, the total electron charge detected by the CCD was found to be linear with tube current. The total charge is a reliable quantity since is does not depend on any event selection criteria. The data are presented in the next subsection.

1.4.3.1 Determination of $\hat{\epsilon}$ and ϵ

An example of experimental pileup data is shown in Figs. 1.23 - 1.26. The CCD w203c2 was used with a 7 second exposure on all 12 x-ray targets. The data for each target is presented with two graphs forming two columns . The left hand column plots the number of detected counts in the K_α per frame per quadrant and is normalized to the x-ray tube current (in units of μA) versus the x-ray tube current. The counts are determined by fitting a three parameter gaussian curve to the K_α peak and using the fitted coefficients to determine the total counts. The four grade selections displayed are G0 (triangles), G0234 (stars), G02346 (squares), and G01234567 = All (diamonds). The value for each quadrant is plotted independently. The lines result from a least squares polynomial fit to Eqn. 1.16. The fit for each quadrant is plotted independently. The zero current intercept averaged for all four quadrants is listed in the first column within each figure, and the zero current slope is listed in the second column. The third column is the slope normalized by the square of the intercept and multiplied by 10^5, which is called the rate. This number provides a configuration-independent slope which only depends on the number of detected x-rays, not on the x-ray tube current. The units for the rate are $(\mathrm{Counts/Frame/Qd})^{-1}$. The fourth column displays the error for the rate.

In an ideal detector with no pileup effects, a horizontal lines would result. The non-zero slope of all the lines clearly indicates the presence of pileup. The presence of a non-linear slope for high Z indicates higher order pileup events, for which the quadratic correction of Eqn. 1.16 becomes important.

In the righthand column are similar plots for the number of pixels above the threshold (diamonds) and the total charge collected (triangles). Printed underneath the values of intercept and slope are the respective errors. The fact that the normalized charge doesn't vary significantly with x-ray tube current is good evidence for linearity of the x-ray flux with tube current.

Figures 1.27 and 1.28 are parallel to Figs. 1.23 - 1.26, except the analysis uses *all* x-rays in the spectrum, not just those in the K_α peak. A useful number from these plots is the intercept value from a linear fit to the x-ray fluxes from all grades. From this number the pileup-corrected branching ratios can be computed.

For our pileup analysis, the most significant number presented in each figure is the rate and error for the G02346 grade set, the set used most commonly for the ACIS calibration. These figures were produced for all 11 test configurations, although the other 10 configuration's figures are not included for space reasons. A summary for the G02346 rate values for all configurations is presented in Figs. 1.29 and 1.30. Figure 1.29 shows the rate for the first targets elements. The graph for each target shows the rate value with errors for each test configuration. Not every configuration has a value for every element since due to some experimental problems and time constraints. A mean value has been determined for the front sided data (i.e. not including w140c4r), excluding any suspicious data points. The mean value is plotted as the horizontal dashed line and is printed in the upper right of each figure. Figure 1.30 corresponds to Fig. 1.29, but shows results for the other six targets.

Figure 1.31 presents a summary of the mean rate values, both as a function of the K_α energy (top) and the x-ray penetration length (bottom) in silicon. With the exception of the Cl line at 2621 eV, the rate is roughly a constant at low energies, and increases quickly at high energies. The Cl line is a known exception since the target source is actually KCl and the K line competes with the Cl, causing more relative pileup than the other targets.

An example of pileup corrections for an ACIS CCD is shown in Table 1.22. Typical detected flux rates for the CCD w215c2r (which presently is located in the I3 position of the ACIS flight focal plane) are listed in the second column for the 13 different K_α x-rays listed in the first column (Mn K_α has now been included, whose source is radioactive Fe^{55}).

The third column lists the mean values for $\hat{\epsilon}$ presented in Figs. 1.29 and 1.30. The fourth column lists the corresponding incident fluxes as determined by Eqn. 1.16, and the next column is the ratio N_i/N_d. These measurements were conducted with a 3.28 s exposure time. The last column lists the corresponding ratio if a 7.15 second exposure time had been used for the same incident flux.

K_α X-ray	Detected Flux	$\hat{\epsilon}$	Incident Flux	Correction Factor	Correction Factor
	(G02346)	(10^5)	(G02346)	(3.28 sec)	(7.15 sec)
Al	1145	6.69	1246±15	1.088	
Si	1310	4.88	1404±17	1.072	1.186
P	1120	7.15	1225±13	1.094	1.257
Cl	605	11.1	651 ±6	1.076	
Ti	1285	4.62	1370±8	1.066	1.169
V	1180	4.57	1251±8	1.059	
Mn	880	7	938±6	1.060	1.174
Fe	1040	8.07	1143±10	1.099	
Co	950	10.3	1062 ±11	1.118	
Ni	840	13.5	959 ±19	1.142	
Cu	700	18.2	815 ±22	1.164	1.643
Zn	660	26.4	829 ±46	1.256	
Ge	480	46.9	662 ±87	1.379	

Table 1.22: Example of pileup correction factors for typical detection fluxes in w215c2r

The previous analysis is directly specific to the spectra emitted by HEXS. That is, $\hat{\epsilon}$(E) includes all the effects of spectral impurities particular to the HEXS source. While this is useful for computing pileup effects on HEXS data, a more general analysis requires ϵ, which is independent of the spectra. Equation 1.13 gives the relation between $\hat{\epsilon}$ and ϵ in terms of α (the number of bad events per good event) and $\epsilon^{'}$ (the average ϵ associated with the "out-of-band" portion of the spectrum). Mathematically, a direct solution for ϵ(E) from the 12 different energies is complicated since $\epsilon^{'}$ depends on ϵ, and we use an iterative approximation described as follows. Using interept values for G02346 and G01234567 from the left hand column in Figs. 1.23 - 1.28, we compute f_B or α. Plots of α for each target from every data set are presented in Figs. 1.32 and 1.33. Using initial guesses for ϵ, spectrally averaged values of $\epsilon^{'}$ are computed. Together with α, new values of ϵ are generated according to Eqn. 1.13, and the process is repeated until the values become self-consistent. Plots of $\epsilon^{'}$ for all targets and data sets are shown in Figs. 1.34 and 1.35.

Figures 1.36 and 1.37 display the final values of ϵ, as computed by Eqn. 1.13. These values of the pileup cross section as a function of energy for a monochromatic incident beam, which are summarized in Fig. 1.38, represent the major result of the pileup experiments.

Notice that the low energy values are close to the theoretical minimum of $\epsilon = 3.4 \times 10^{-5}$. Recall this value corresponds to a cross-sectional area of 9 pixels in one quadrant (viz, 9/262144). We do not yet understand why the value of ϵ has a slight increase at the lowest energies. The discrepancy is no more than about one standard deviation. A comparison with Fig. 1.32 suggests that spectral impurities may be the cause since the 1740 eV Si point (which is most spectrally pure) lies near the minimum while the 2622 eV Cl point (which is most spectrally impure due to a potassium line) lies far from the minimum. The 1487 eV Al source is also known to be very spectrally impure.

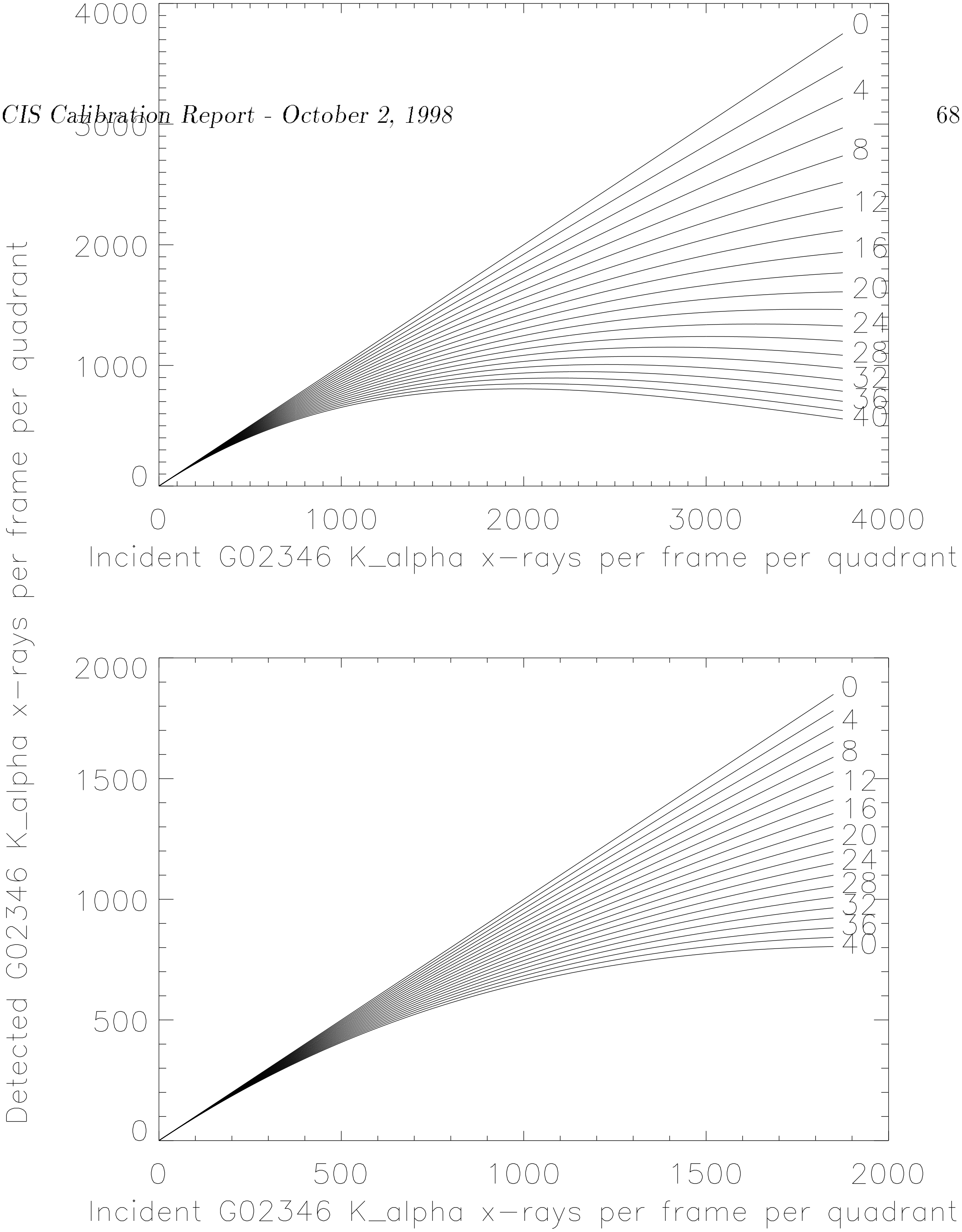

Figure 1.22: Predicted relationship between detected and incident flux parameterized by the assumed value of $\epsilon \times 10^5$. For example, the curve labeled 4 is the prediction for $\epsilon = 4 \times 10^{-5} = 10.5$ pixels.

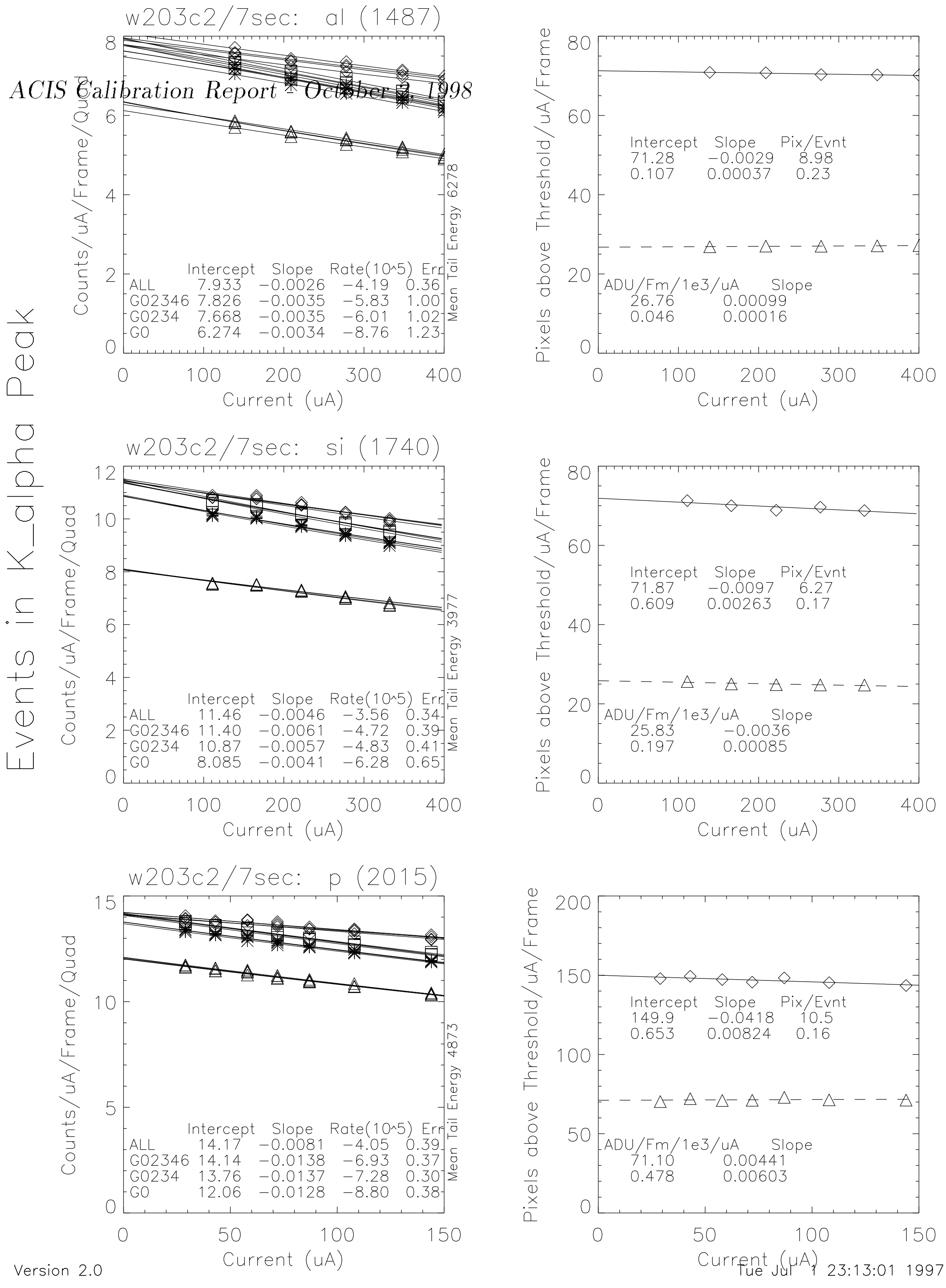

Figure 1.23: Raw HEXS pileup data for for detector w203c2 with a 7 second exposure for characteristic K lines from Al,Si, and P targets, with best-fit model for various ASCA event grade sets. triangles:G0; stars:G0234; squares: G02346; G01234567: diamonds. Points for each detector quadrant are shown. Best-fit model parameters are shown in each panel. See text for details.

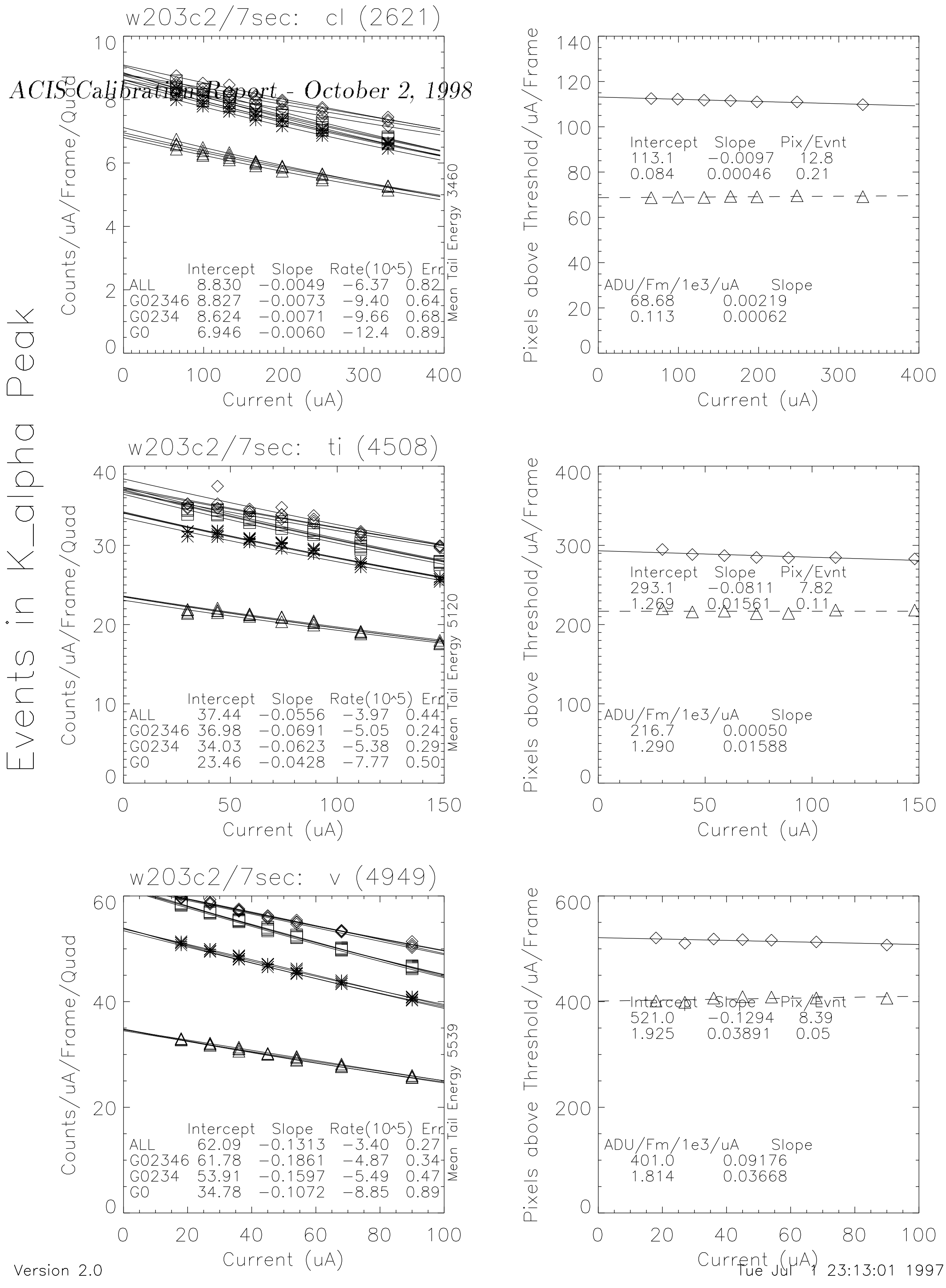

Figure 1.24: Raw HEXS pileup data for K_α for detector w203c2 with a 7 second exposure for characteristic K lines from Cl,Ti, and V targets, with best-fit model for various ASCA event grade sets. triangles:G0; stars:G0234; squares: G02346; G01234567: diamonds. Points for each detector quadrant are shown. Best-fit model parameters are shown in each panel. See text for details.

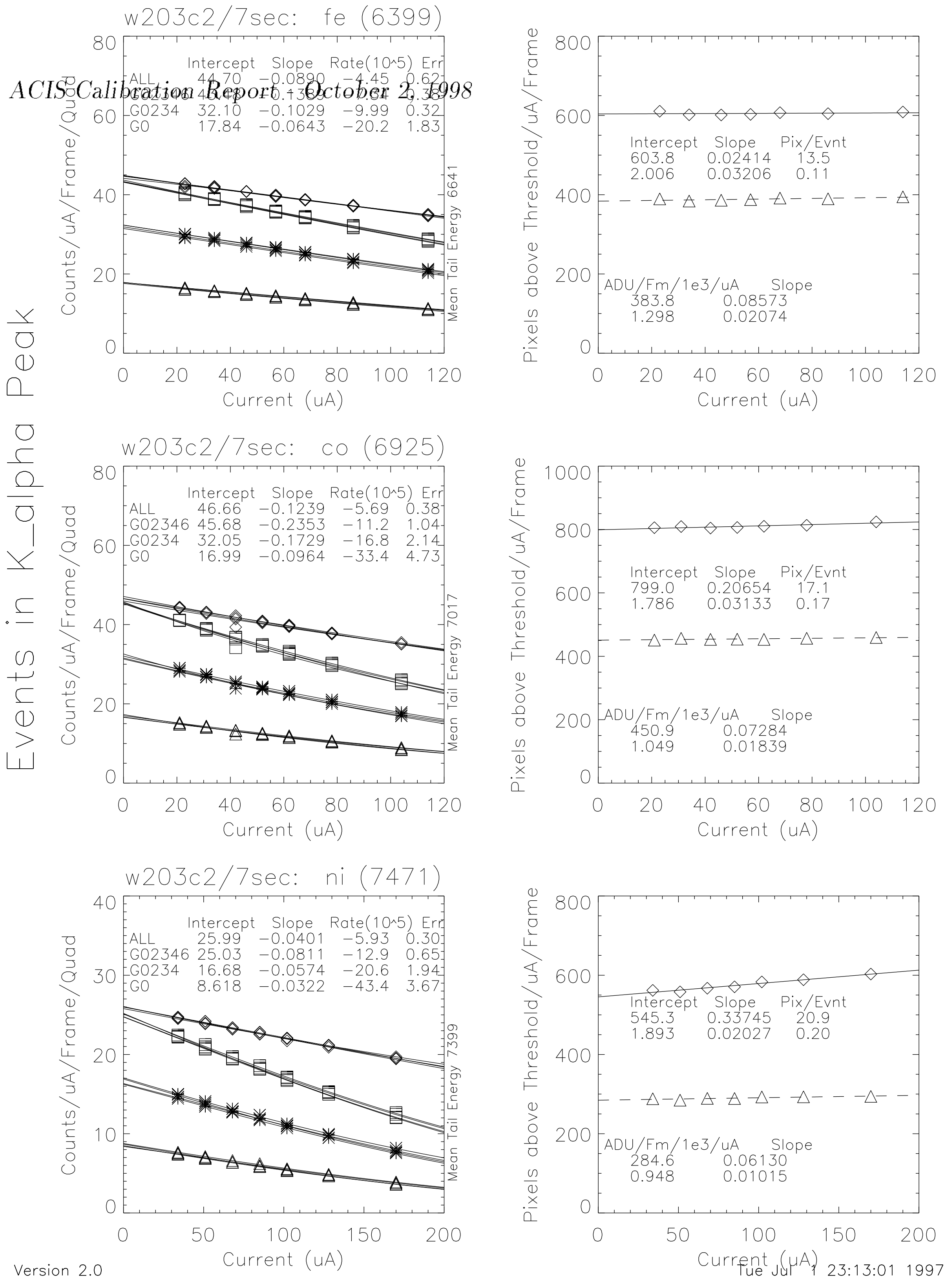

Figure 1.25: Raw HEXS pileup data for K_α for w203c2 with a 7 second exposure for Fe,Co, and Ni targets

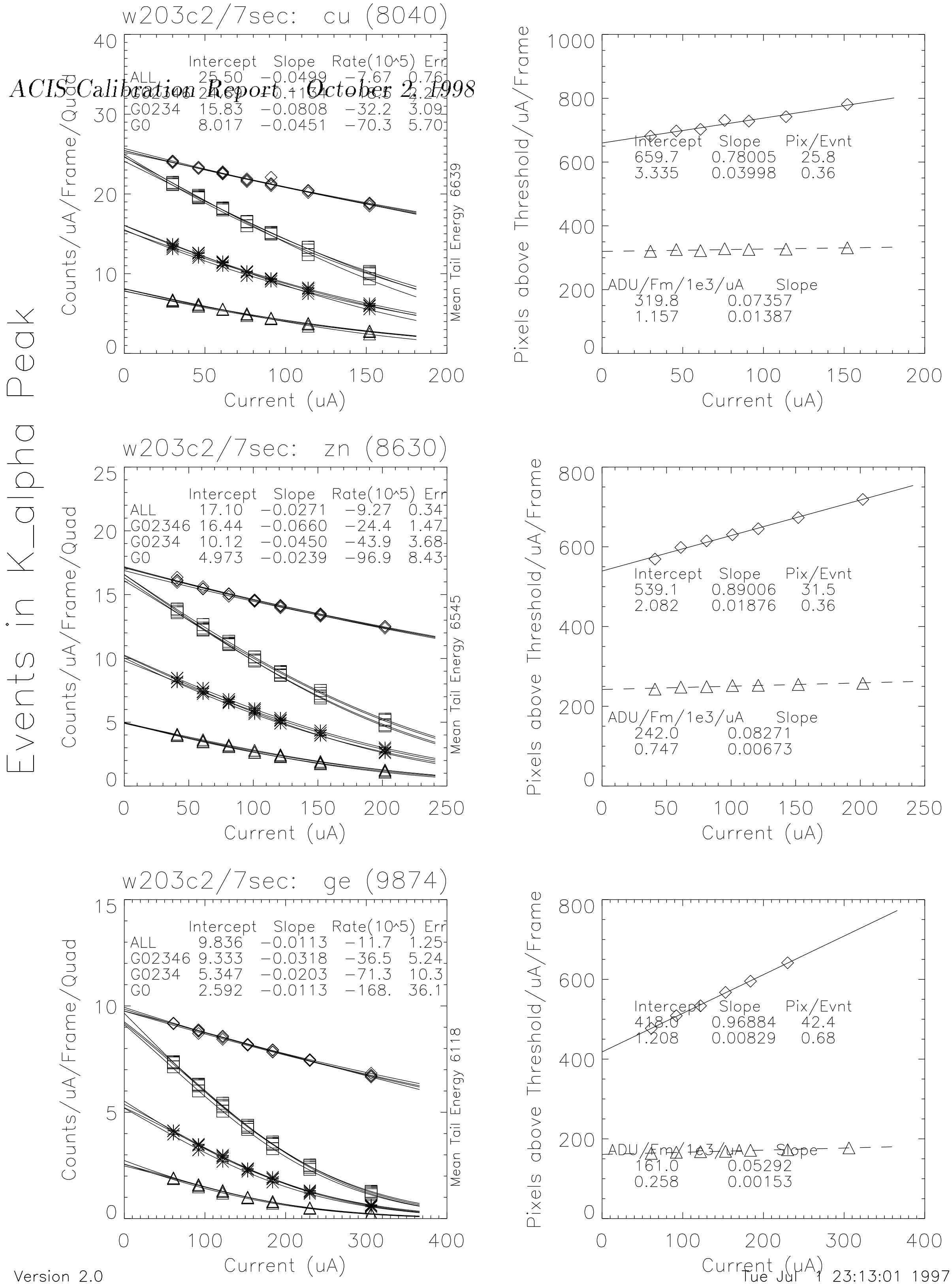

Figure 1.26: Raw HEXS pileup data for K_α for w203c2 with a 7 second exposure for Cu ,Zn, and Ge targets

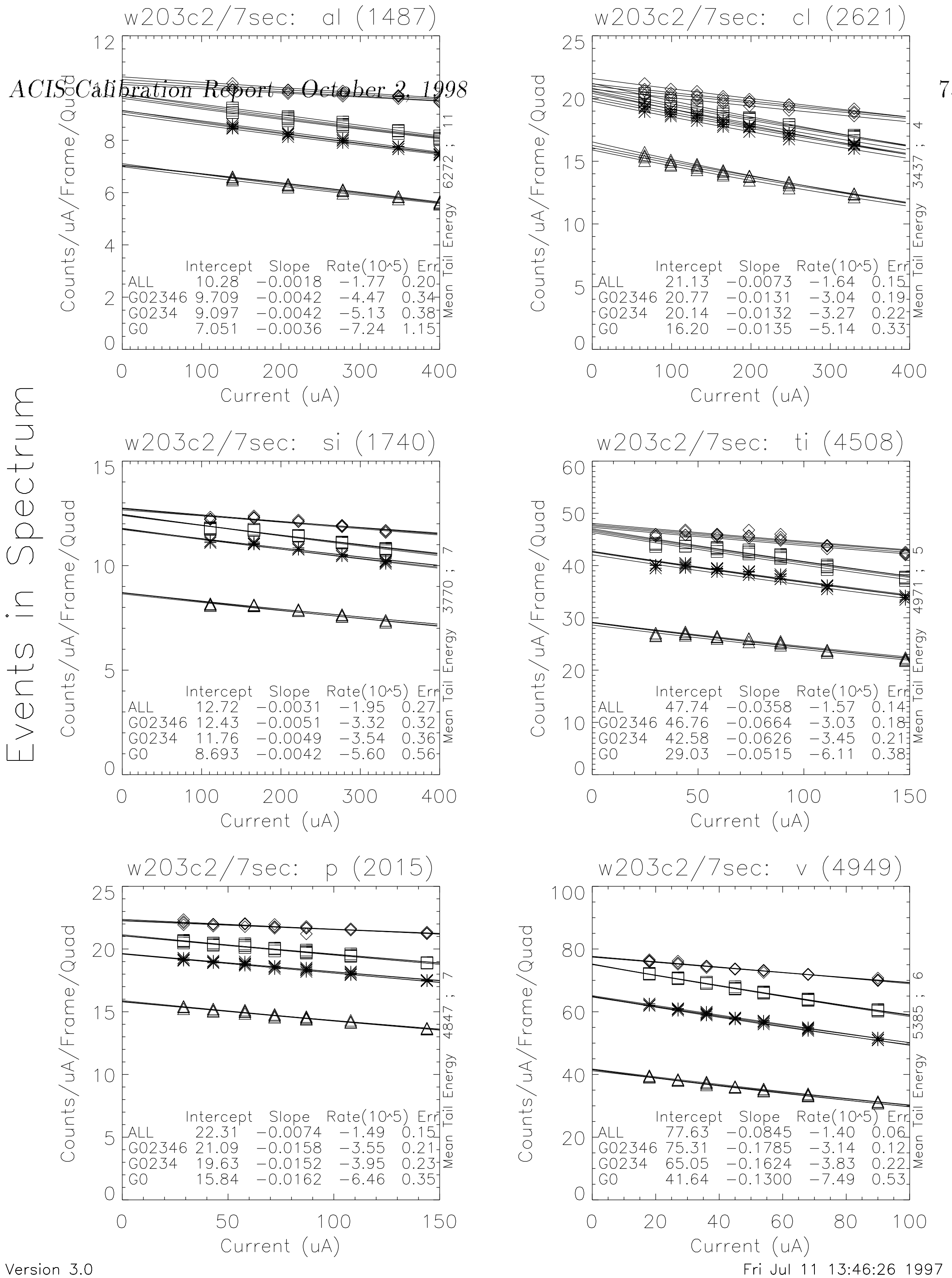

Figure 1.27: Raw HEXS pileup data for entire spectrum for w203c2 with a 7 second exposure for Al, Si, P, Cl,Ti, and V targets

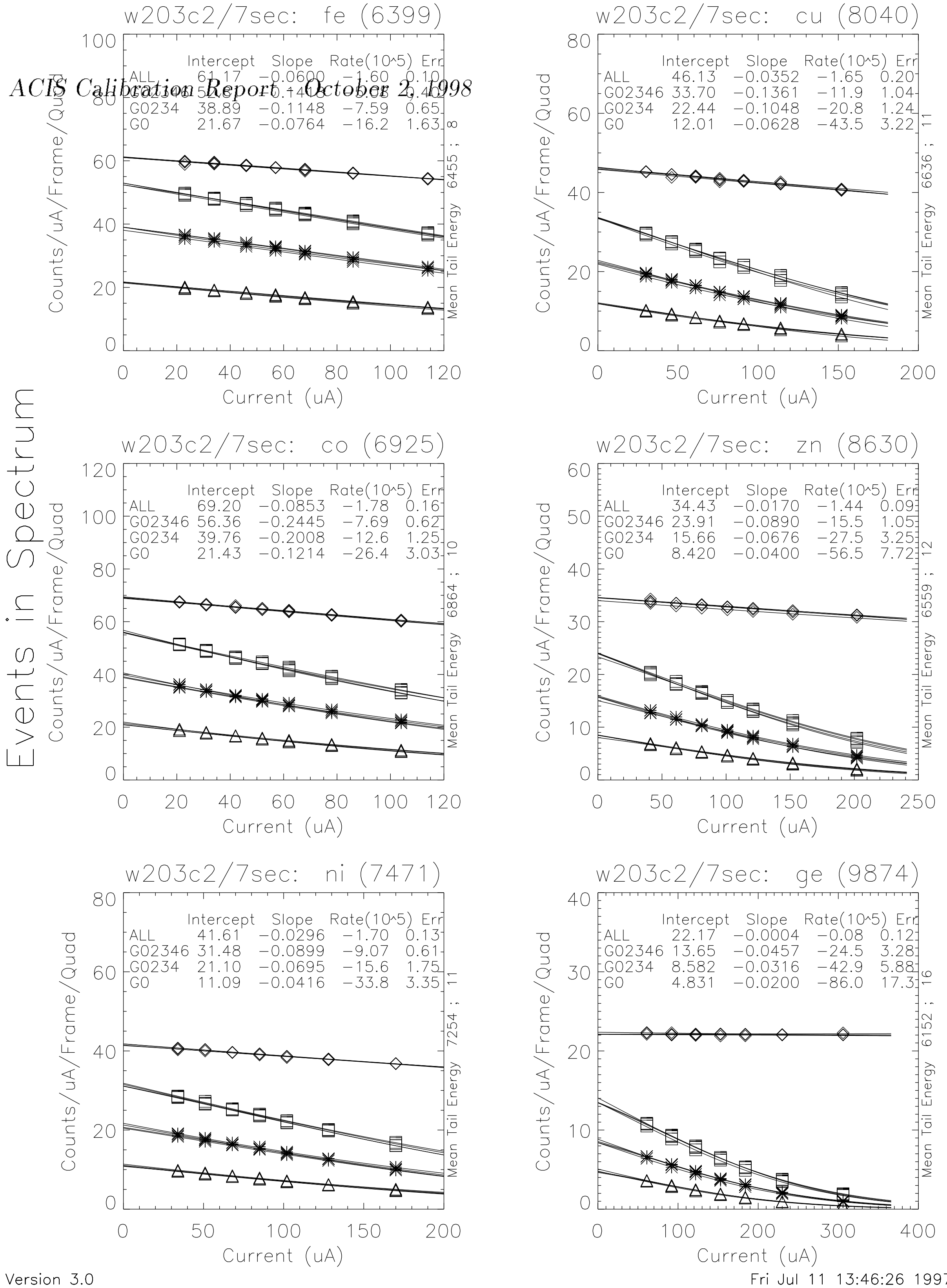

Figure 1.28: Raw HEXS pileup data for entire spectrum for w203c2 with a 7 second exposure for Fe, Co, Ni, Cu, Zn, and Ge targets

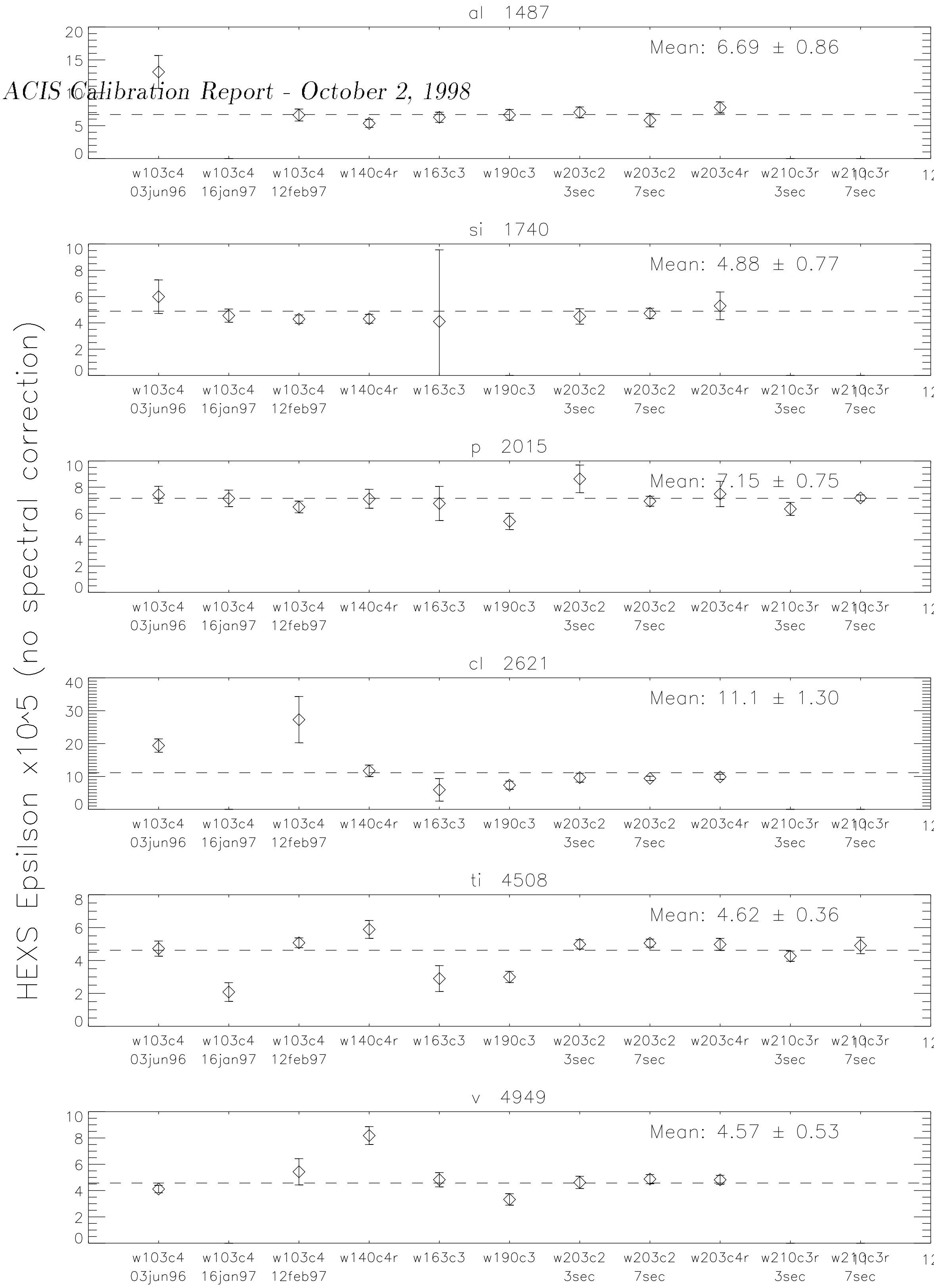

Figure 1.29: Mean g02346 epsilon for all data sets with no spectral correction (Al - V)

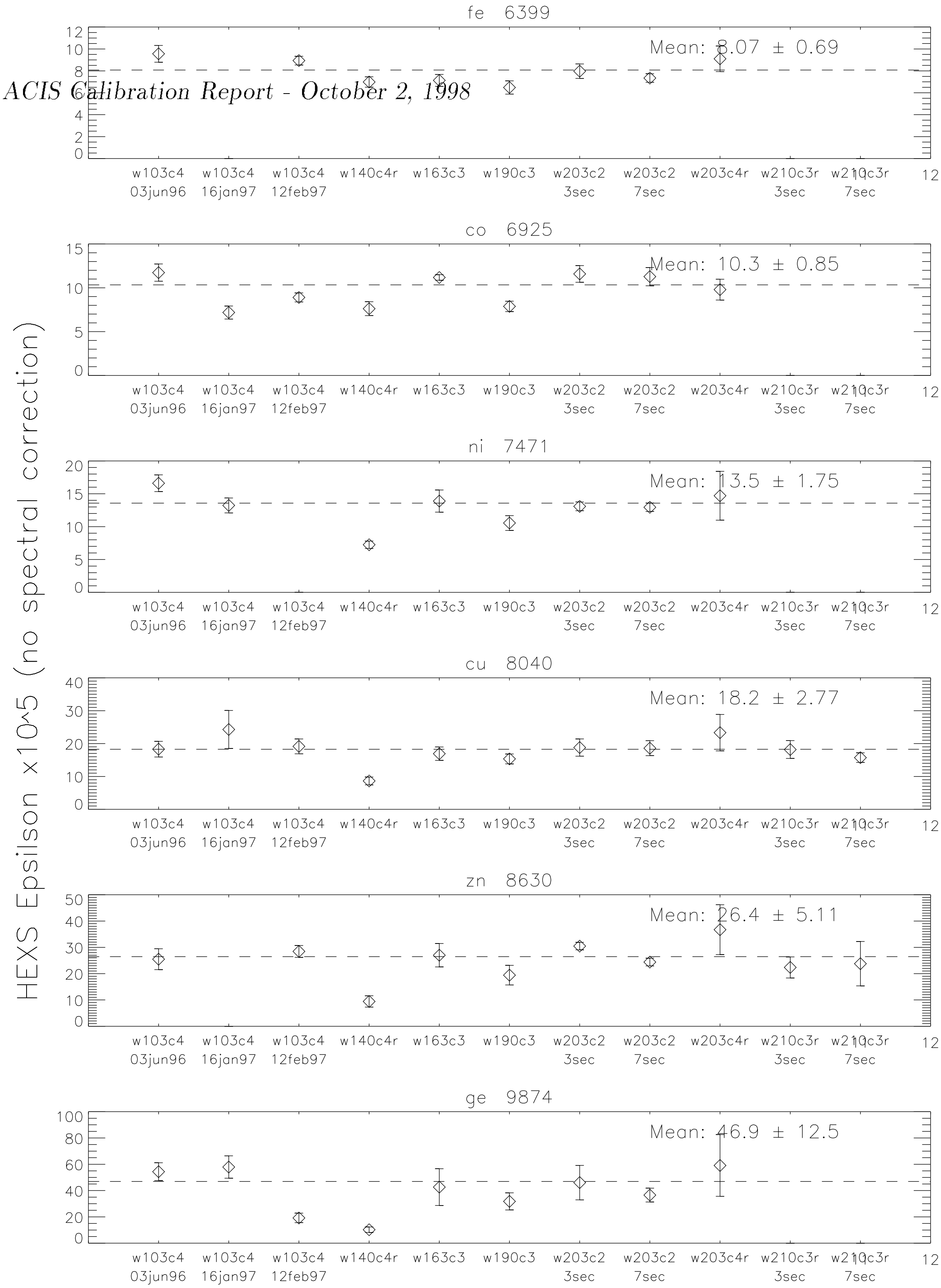

Figure 1.30: Mean g02346 epsilon for all data sets with no spectral correction (Fe - Ge)

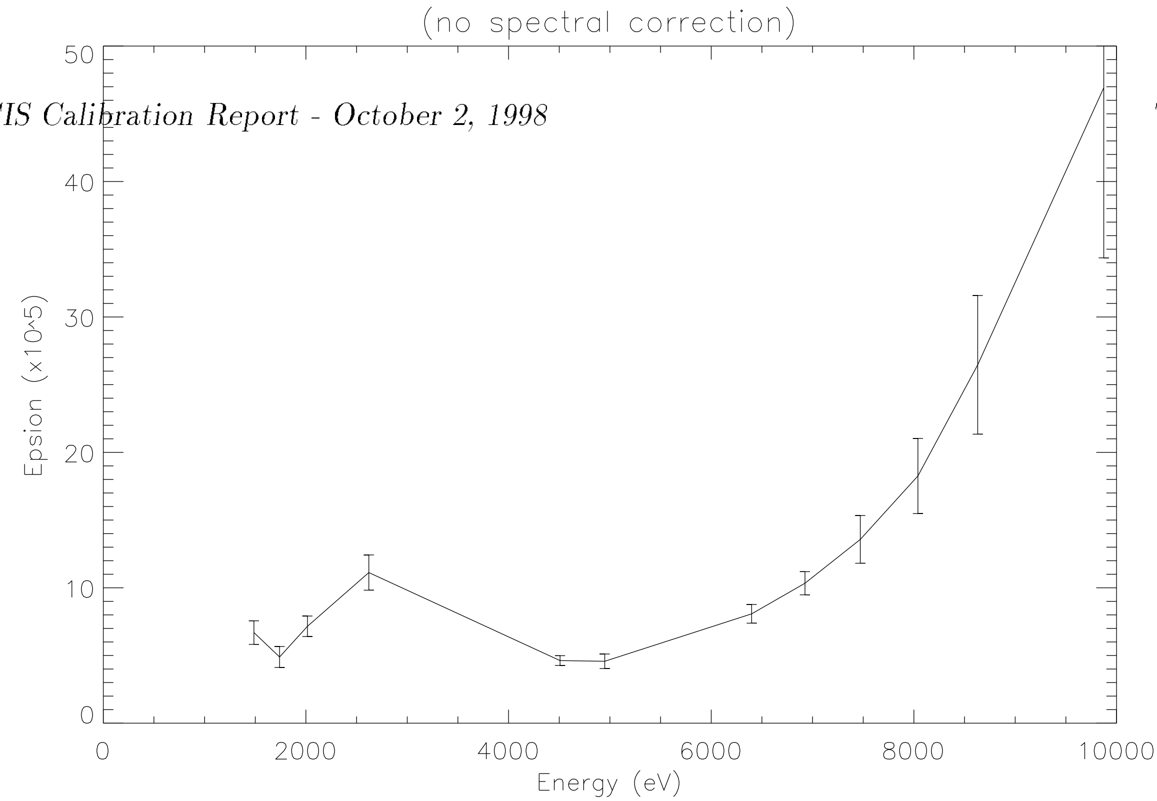

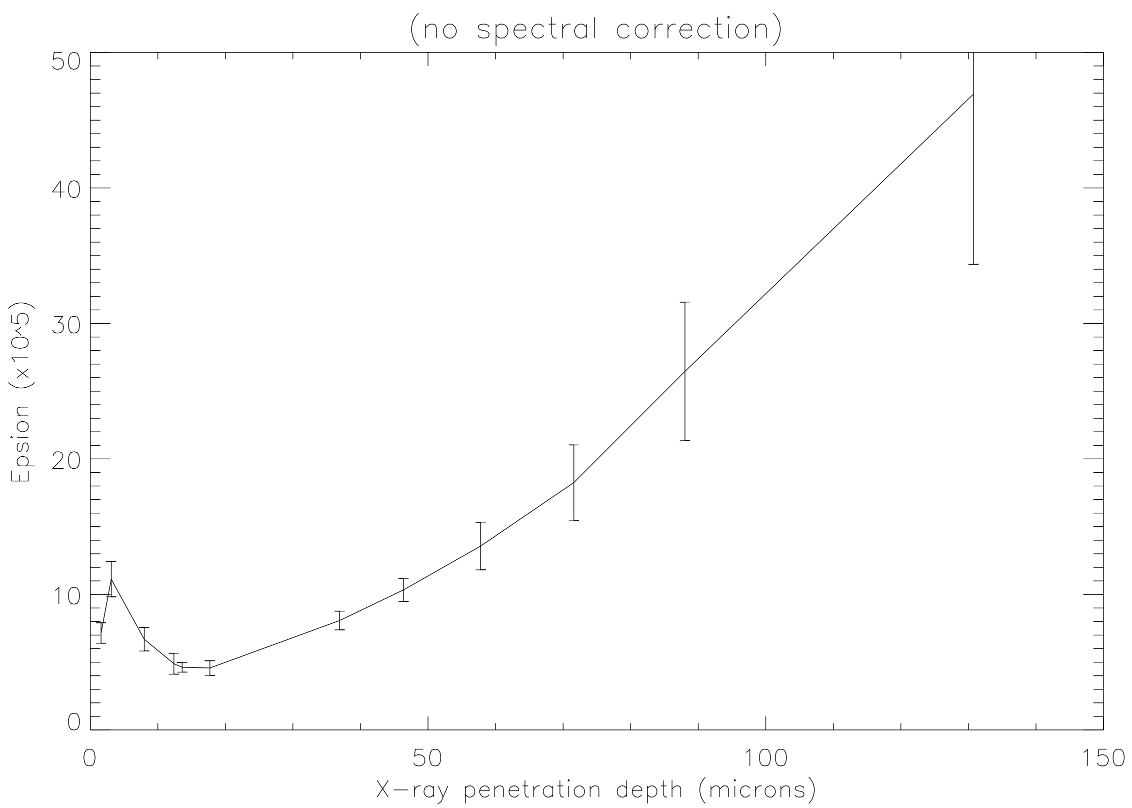

Figure 1.31: Variation of epsilon with for raw HEXS data

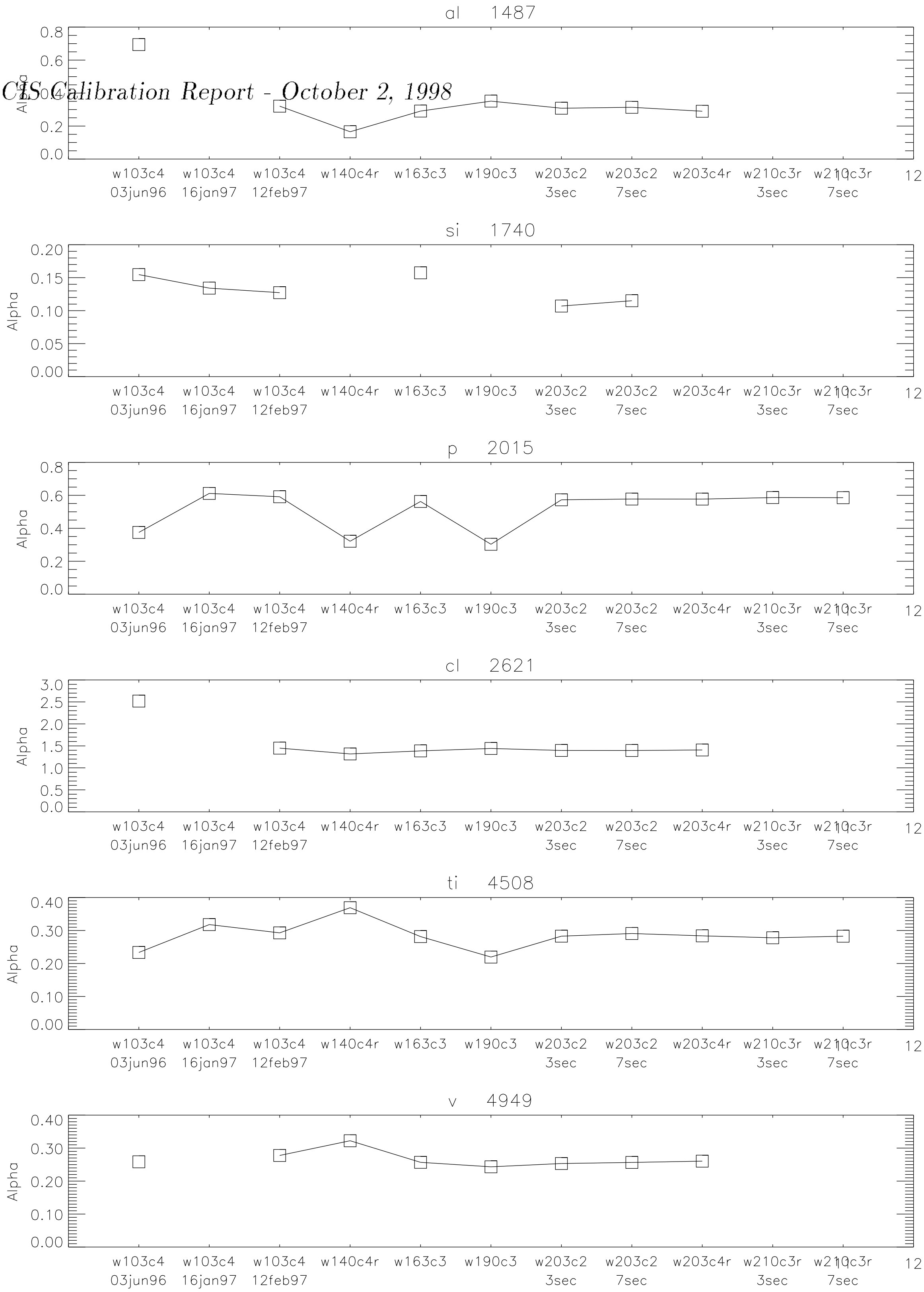

Figure 1.32: Variation of alpha, the ratio of bad to good x-ray events, for Al to V

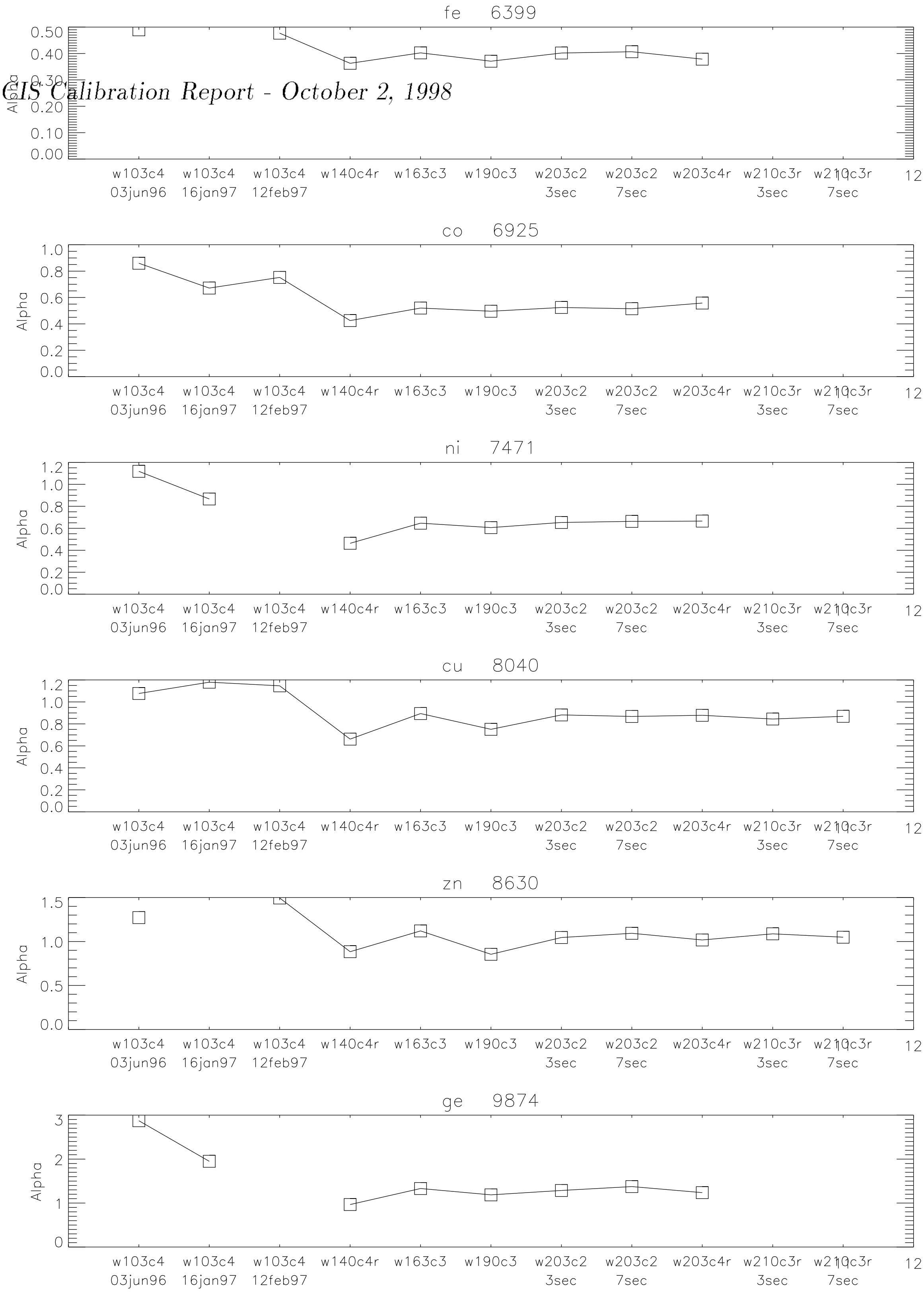

Figure 1.33: Variation of alpha, the ratio of bad to good x-ray events for Fe to Ge

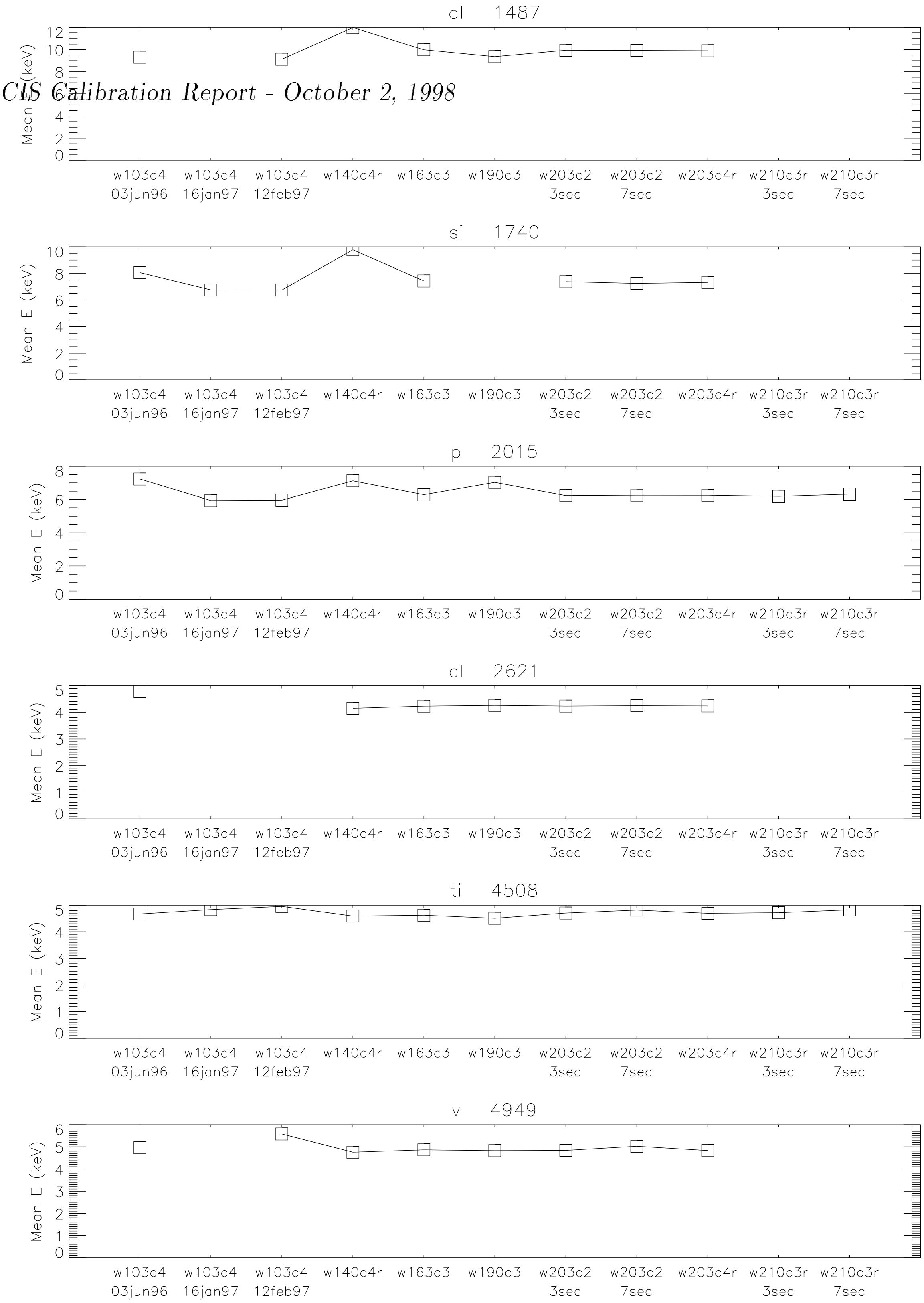

Figure 1.34: Variation of spectrally averaged epsilon (ϵ') for Al to V

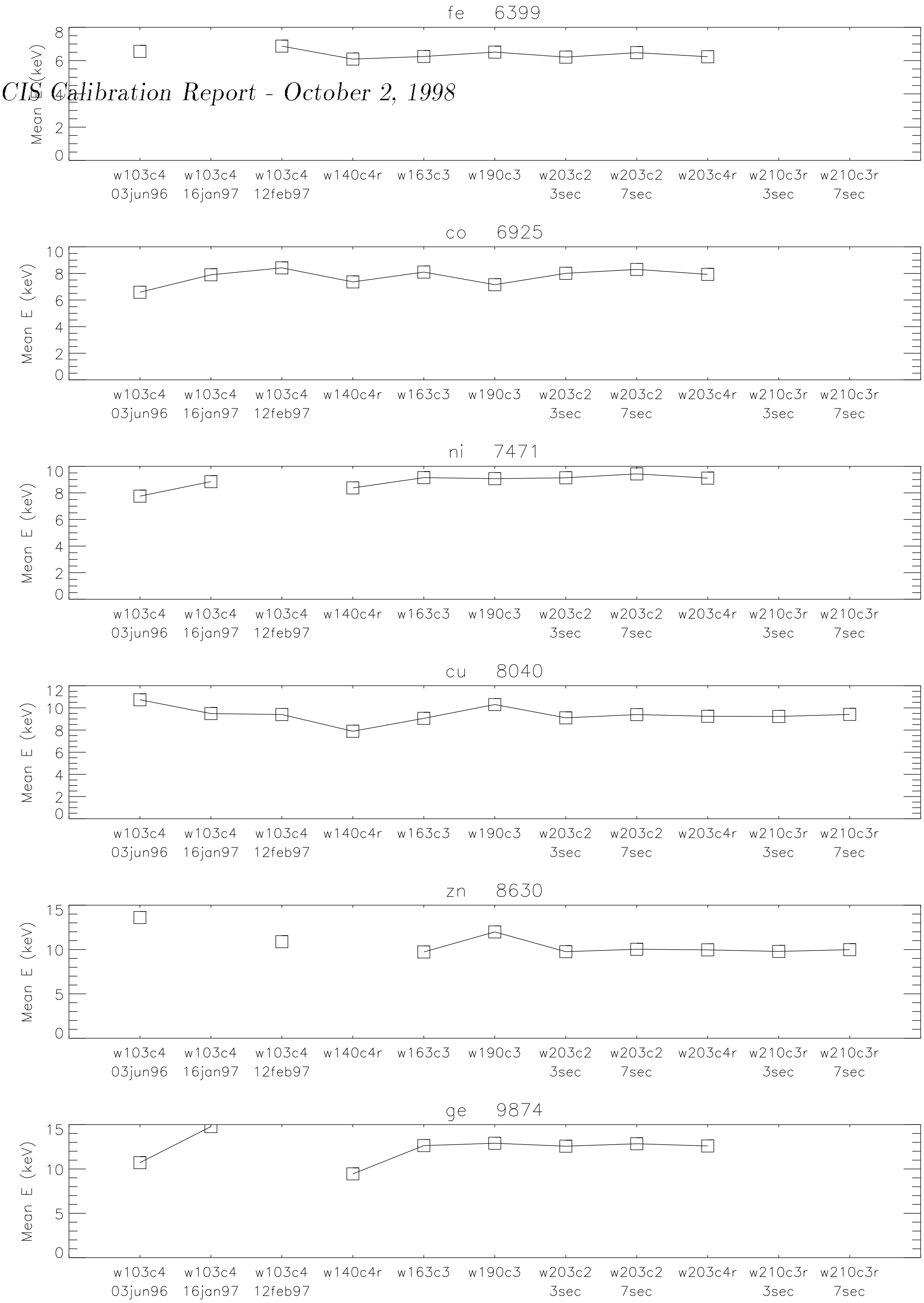

Figure 1.35: Variation of spectrally averaged epsilon (ϵ') for Fe to Ge

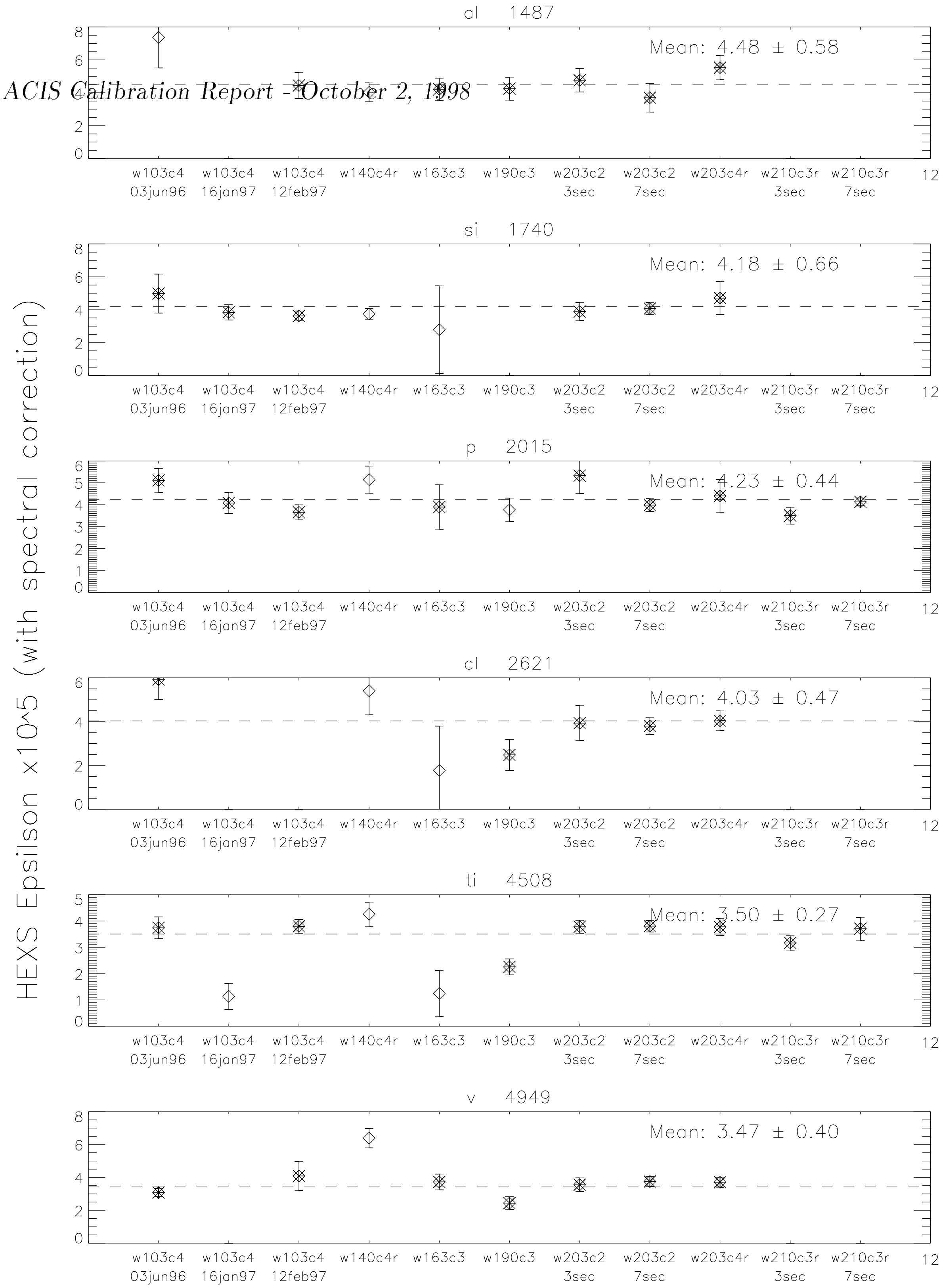

Figure 1.36: Mean g02346 epsilon for all data sets including a spectral correction

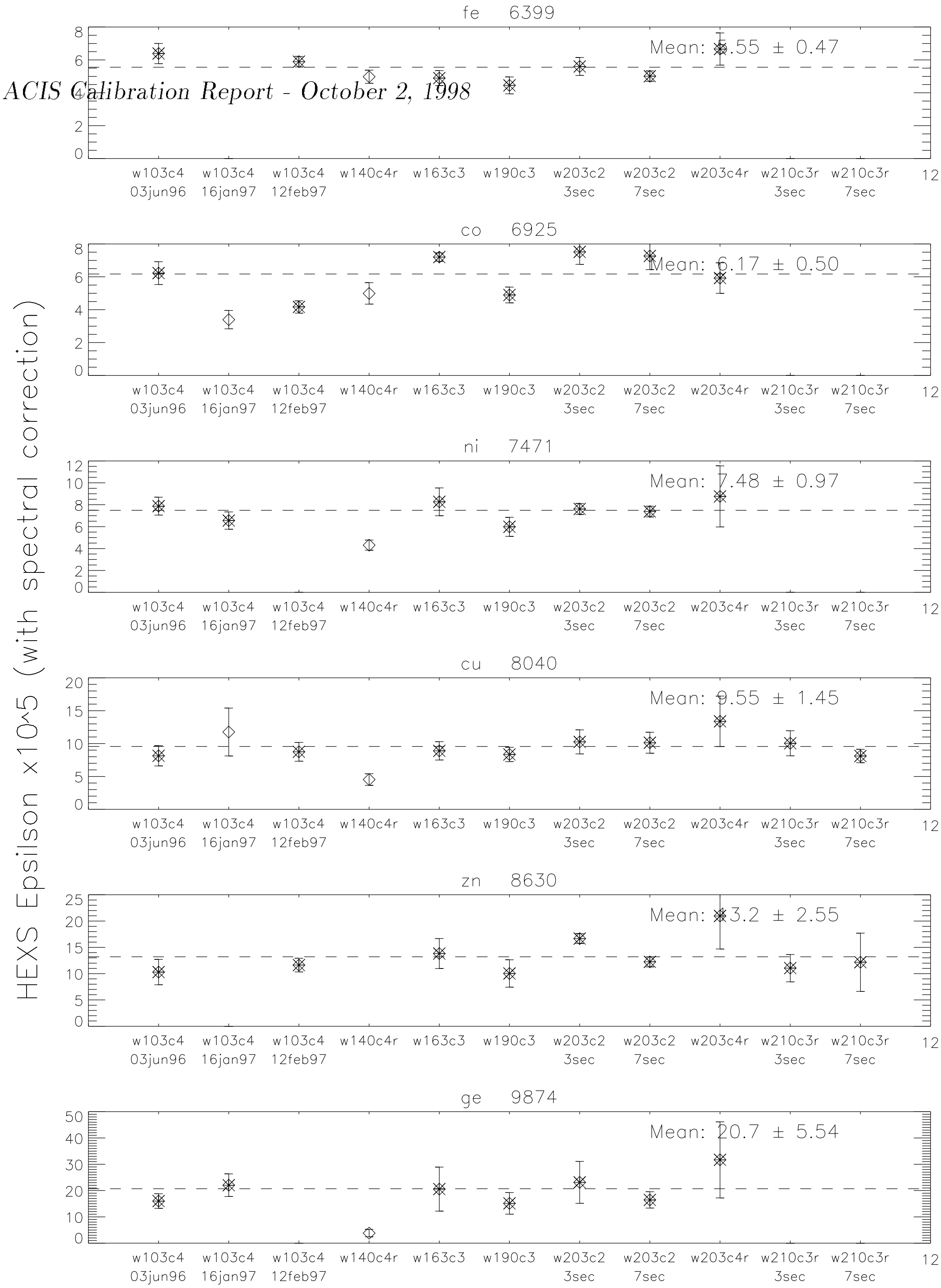

Figure 1.37: Mean g02346 epsilon for all data sets including a spectral correction

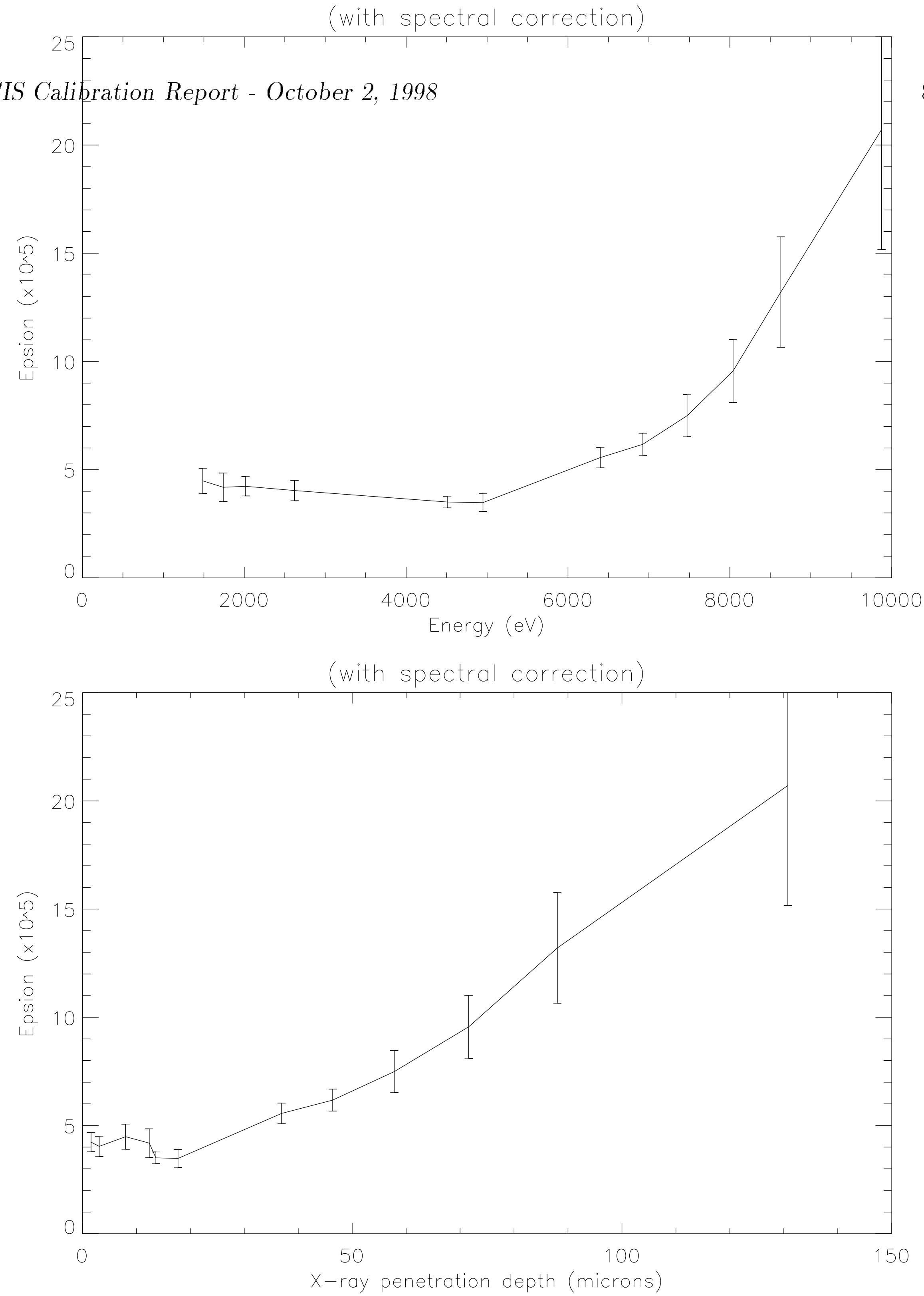

Figure 1.38: Variation of epsilon including corrections for spectral impurities

1.4.4 Redistribution of X-rays by Pileup

Pileup can effect event detection in two ways, event-extinction and event-redistribution. Up to this point, only event-extinction has been modeled since its occurance rate is nearly a factor of ten less than event-redistribution. This difference is nicely displayed by reanalyzing the experimental pileup data from section 3 as follows. For a series of energy spectra at different source fluxes (i.e. different x-ray tube currents), the spectra are normalized to the total exposure time and incident flux. Since the CCD output electronics use an A to D converter, the energy scale is discretized into intervals. For each energy interval, a plot is made of the spectral intensity versus the incident flux. If there was no pileup effect, the points would lie along a horizontal line, that is the normalized spectral intensity would not vary with incident flux at that energy. For weak pileup in the linear regime, the points actually lie on a linear line with a negative slope. In effect, this procedure results in plots similar to Figs. 1.23 - 1.26, except now there is a plot for every energy bin (in our case there were 4096 energy bins). The intercept of this line represents the intensity observed at that energy if pileup effects did not occur. Plotting all 4096 intercepts together versus energy results in a new spectrum which can be considered the spectrum observed if the detector had no pileup effects. Correspondingly, in addition to the intercept, the slope of each line represents a quantitative measure of the pileup effect at that energy. Plotting all 4096 slopes together versus energy results in a new spectrum reflecting the spectral change caused by pileup.

Figures 1.39 - 1.40 show the spectral change for all 12 energies as observed by w203c2 during 7 second exposures. The most prominant feature for each (target) energy is the large negative spike which represents x-ray extinction of the K_α peak. For example, in V, the K_α line at 4949 eV looses about 0.02 x-rays/μA^2 in each energy bin. Associated with each K_α extinction spike is the K_β extinction spike, usually about ten times smaller. Small negative spikes also result from the Si escape peak, the fluorescence peak, and the L peak (best seen in spectra from higher Z, e.g. Cu). Aside from negative extinction spikes, there are positive redistribution spikes. The largest such positive peak always occurs at twice the K_α energy. This peak represents the pileup of two K_α x-rays such that they appear as a single x-ray at twice the energy. One nice example of additive redistribution is the Cl plot which shows a series of three positive peaks, each representing pileup from all three combinations of K_α and K_β x-rays. Redistribution in the continuum can also be seen, but is too small to be observed on the displayed scale. These events represent the slight overlap of two x-rays appearing as one x-ray, but without the total inclusion of the sum all their charges (or energy). The collected energy lies anywhere between that of one memeber of the incident pair of x-rays and that of the sum of the pair. The number of these redistributed "continuum" events is a small fraction (about 10%) of redistributed events with no energy loss. This observation forms an important conclusion: the largest effect of spectral redistribution is the simple energy summation of two x-rays.

Other minor redistribution effects are observed around the base of the K_α peak. The net effect appears as a slight line shift, caused by pileup moving a few events from the low energy side of the K_α peak to the high energy side. However, this detail was not regularly oberved under all conditions.

1.4.5 Branching Ratio Variation with Flux

Branching ratios can be defined as the number of x-rays detected in one grade selection divided by the total number of x-rays detected. The branching ratio is not only energy dependent but is flux dependent. The laboratory pileup data can be used to compute the effect of flux on the branching ratios. These "branching ratio epsilons" are presented in Figs. 1.41 and 1.42, which show some variation between the various CCDs. These numbers are relative correction factors to the branching ratio per detected g02346 x-ray per quadrant. For example, if the BR eps equals 4×10^{-5}, and there are 1000 x-rays per quadrant per frame, then the relative correction to the branching ratio is 4%. The numbers in Figs. 1.41 and 1.42 are specfically the number of G02346 events in the K_α peak divided by all events in the peak. The effect of pileup on branching ratio has a direct effect on methods which use the branching ratio to determine the depletion depth. An example of this method is discussed in section 1.6.2.

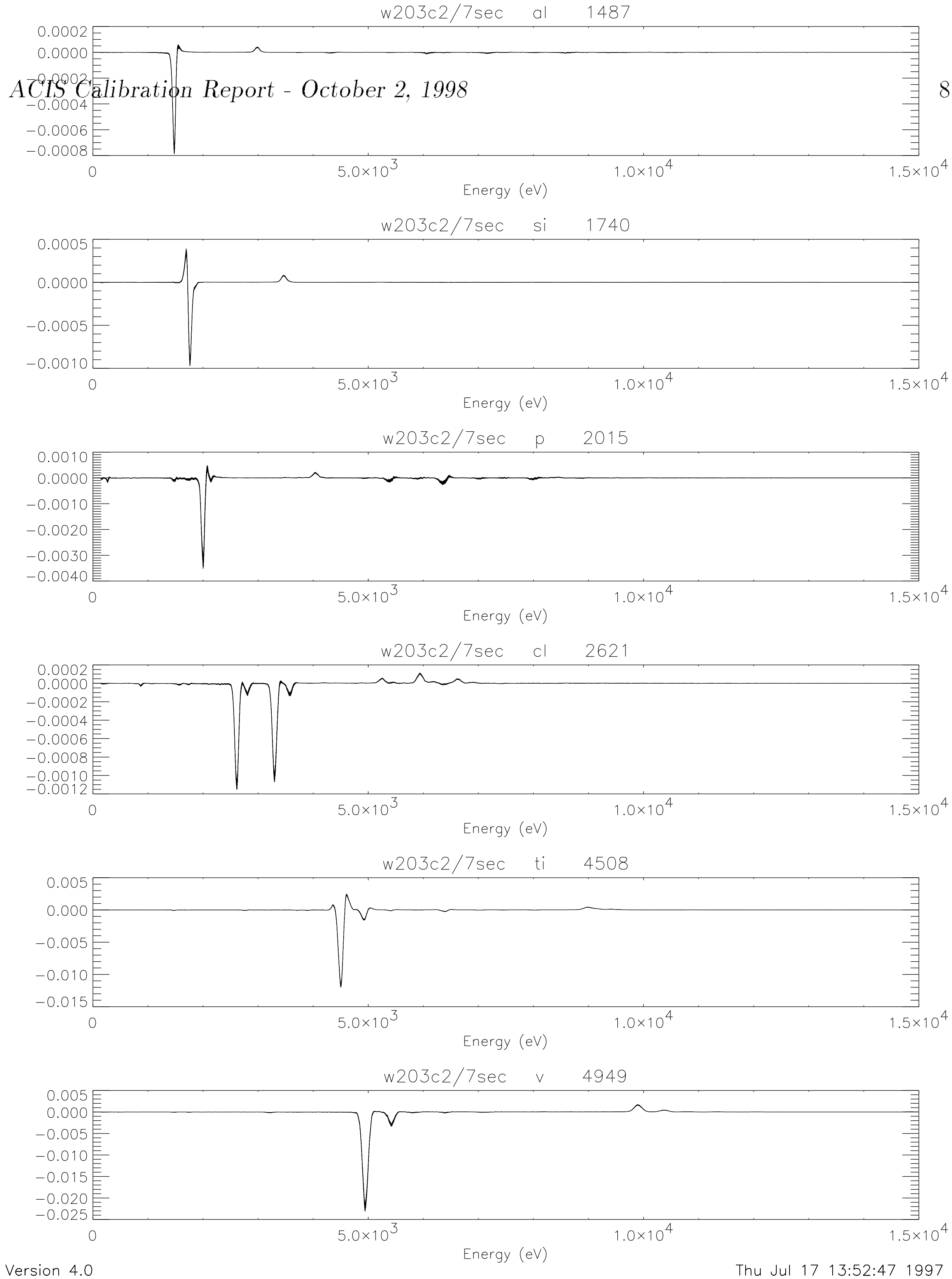

Figure 1.39: Redistribution of G02346 events in w203c2 during 7 second exposures due to pileup for Al, Si, P, Cl, Ti, and V HEXS targets

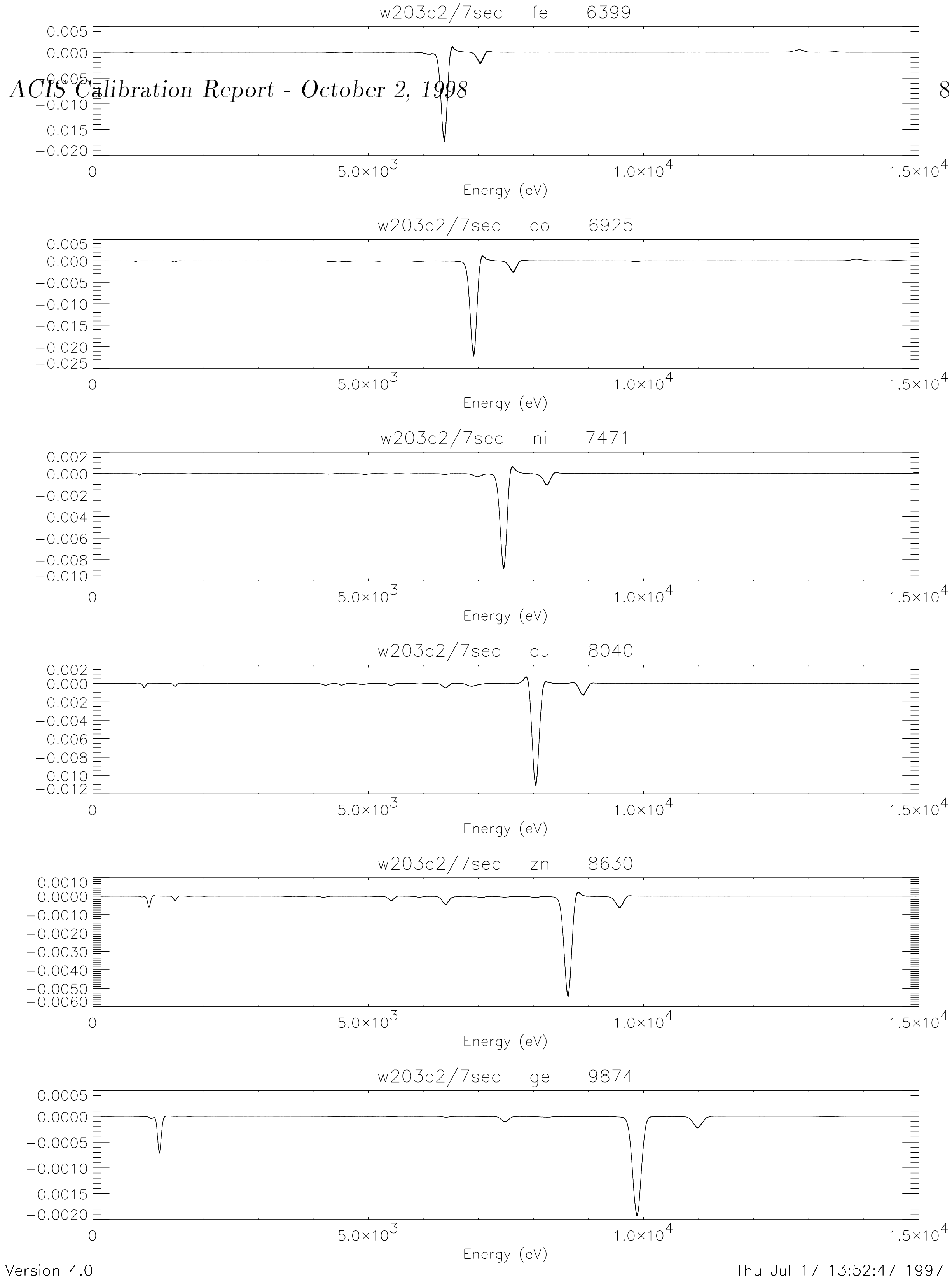

Figure 1.40: Redistribution of G02346 events in w203c2 during 7 second exposures due to pileup for Fe, Co, Ni, Cu, Zn, Ge HEXS targets

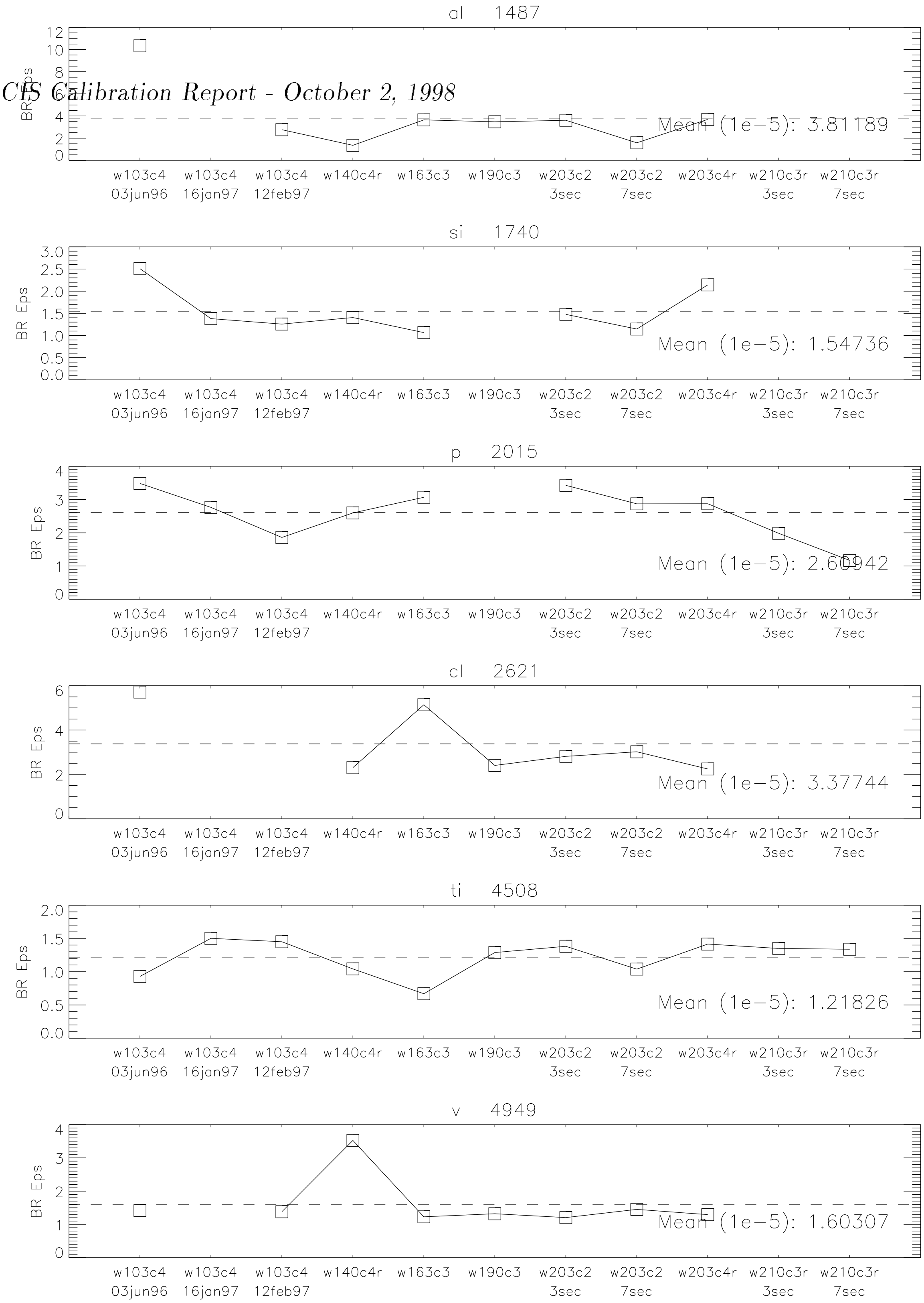

Figure 1.41: Branching ratio epsilons from data set for elements Al - V

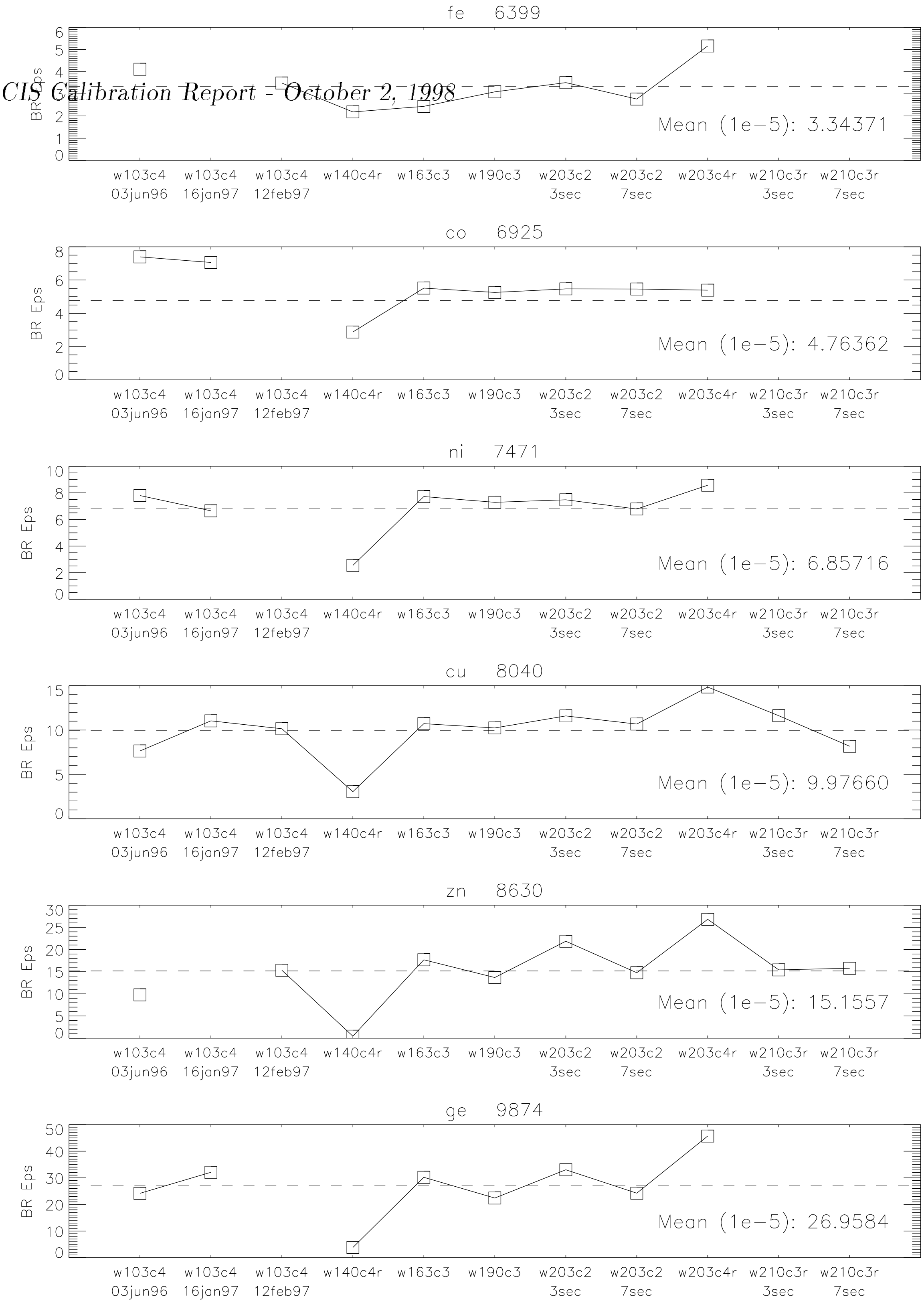

Figure 1.42: Branching ratio epsilons from data set for elements Fe - Ge

1.4.6 Single Pixel Pileup

As an imaging x-ray telescope, AXAF focuses a point source onto the CCD. Since the point response function FWHM is comparable to the size of one pixel, pileup from a strong point source is a particular problem.

All pileup cross sections presented so far are evaluated in terms of detected x-rays per quadrant per frame. However, it is often useful to describe pileup in units of x-rays per pixel per frame. The factors are translated multiplying ϵ by $256 \times 1024 = 2.62 \times 10^5$. Thus, if $R_{nopileup}$=incident x-ray rate per pixel per frame for a monochromatic beam, then to first approximation the detected rate $R_{nopileup}$ is given by the transcendental equation

$$R_{pileup} = R_{nopileup} exp\left(2.62 \times 10^5 R_{nopileup} \epsilon\right) \tag{1.17}$$

From another viewpoint, pileup in a single pixel with a monochromatic source is easily understood as a simple Poisson process. That is, if the probability for an x-ray to interact with a pixel during one exposure is λ, then the probability that N x-rays interact during one exposure is

$$P_N = \frac{\lambda^N e^{-\lambda}}{n!}$$

Consider an entire observation of N_{frames} frames. If there was no pileup, the total incident flux of $N_i = N_{frames}\lambda$ x-rays would be detected. The effect of pileup is manifest as several (or many) x-rays which add during one exposure. Let

$$N_0 = N_{nframes} e^{-\lambda} \equiv \text{number of frames with no interaction.}$$

Combining these two equations yields,

$$\frac{N_i}{N_{frames}} = -log\left(\frac{N_0}{N_{frames}}\right)$$

For example, if out of 1000 frames, x-rays from a point source are present in 100 frames, then

$$N_i = -1000 log(900/1000) = 105$$

Thus, pileup accounted for an apparent reduction in the incident flux of 5%.

This method differs from the first method developed in this chapter by treating every incident x-ray as a valid event, including the coincidence of two or many x-rays. This method has use in high pileup situations where Eqn. 1.16 presents ambiguity. For example, the shape of the graphs in Fig. 1.22 show that for a given value of the detected flux, there are *two* possibilities for the incident flux. Without additional information it is impossible to discriminate between the low and high flux solution. Although most astrophysical point sources should not be so strong, the ambiguity of strong sources can be resolved by application of the method described above.